Journal of Volcanology and Geothermal Research, 44 (1990) 189 – 229
Elsevier Sicence Publishers B.V., Amsterdam

Genesis of collision volcanism in Eastern Anatolia, Turkey

J.A. Pearce[a], J.F. Bender[b], S.E. De Long[c], W.S.F. Kidd[c], P.J. Low[d], Y. Güner[e], F. Saroglu[e], Y. Yilmaz[f], S. Moorbath[g] and J.G. Mitchell[h]

[a] *Department of Geological Sciences, University of Durham, Durham DH1 3LE, England*
[b] *Department of Geography and Earth Sciences, University of N. Carolina, Charlotte, NC 28223, USA*
[c] *Department of Geological Sciences, SUNY Albany, Albany, NY 12222, USA*
[d] *Department of Geology, the University, Newcastle upon Tyne NE1 7RU, England*
[e] *MTA Genel, Müdürlügü, 06520 Ankara, Turkey*
[f] *Istanbul Teknik Universitesi, Jeoloji Bölümü Baskanligi, Ayanzaga, Istanbul, Turkey*
[g] *Department of Earth Sciences, University of Oxford, Parks Rd., Oxford OX1 3PR, England*
[h] *Department of Physics, the University, Newcastle upon Tyne NE1 7RU, England*

(Received January 4, 1990; revised and accepted March 23, 1990)

ABSTRACT

Pearce, J.A., Bender, J.F., De Long, S.E., Kidd, W.S.F., Low, P.J., Güner, Y., Saroglu, F., Yilmaz, Y., Moorbath, S. and Mitchell, J.G., 1990. Genesis of collision volcanism in Eastern Anatolia, Turkey. In: P. Le Fort, J.A. Pearce and A. Pêcher (Editors), Collision Magmatism. *J. Volcanol. Geotherm. Res., 44: 184 – 229.*

Late Cenozoic volcanism in Eastern Anatolia extends in a broad SW – NE trending belt across the Arabia – Eurasia collision zone, from the Arabian foreland basin in the southwest and to the Kars Plateau and Lesser Caucasus in the northeast. Foreland volcanism is dominated by basaltic shield and fissure eruptions of transitional tholeiitic – alkaline composition. Volcanism on the thickened crust north of the Bitlis Thrust Zone varies from the mildly alkaline volcano, Nemrut, and older Mus volcanics in the south, through the transitional calc-alkaline/alkaline volcanoes Bingöl and Süphan and the alkaline volcano Tendürek to the calc-alkaline volcano Ararat and older Kars plateau volcanics in the north.

Isotope (Sr, Nd) and trace element systematics indicate that the lavas from the foreland were derived from the mantle lithosphere of the Arabian continent which had been enriched by small volumes of asthenospheric melts over a period of time; and that lavas from the alkaline volcanic area around Mus, and the volcanoes Nemrut and Tendürek north of the Bitlis Thrust Zone were derived from a lithospheric source of similar composition, either from the same, underthrust, Arabian continent or from the Bitlis Massif microcontinent. By contrast, the transitional lavas from Bingöl and Süphan and the calc-alkaline lavas from Ararat and Kars were derived from lithosphere carrying a distinct subduction signature inherited from pre-collision subduction events. Positive correlations between $^{87}Sr/^{86}Sr$ and SiO_2 and Rb/Nb and SiO_2 in the alkaline and transitional lavas suggest that combined assimilation and fractional crystallization was an important process within at least part of the thickened crust of the collision zone. Trace element covariation diagrams such as Y – Rb indicate the importance of hornblende crystallization at depth (and orthopyroxene at shallow levels) within the calc-alkaline provinces, in contrast to the consistently anhydrous crystallization sequences of the alkaline lavas. Trace element diagrams, based on the covariation of compatible and incompatible elements, point to moderate – low degrees of partial melting with residual clinopyroxene throughout, and residual garnet in the foreland province.

Consideration of mineral stabilities, mantle solidi and geothermal gradients before and after collision suggest that lithospheric thickening should both increase the thickness of metasomatized lithosphere and depress the metasomatized zone to greater depths, probably beneath the amphibole and dolomite breakdown curves. Perturbation of the thickened lithosphere by delamination of the thermal boundary layer, perhaps coupled with local stretching associated with pull-apart basins on strike-slip fault systems, is then sufficient to generate melt, the composition of that melt being largely dependent on the enrichment history of the lithosphere in question. In Eastern Anatolia, volcanism appears to have started between about 8 and 6 Ma ago, some 5 Ma after the start of rapid uplift of the East Anatolian Plateau.

0377-0273/90/$03.50

Introduction

Collision volcanism in Eastern Anatolia is thought to have begun in the Late Miocene, as part of a volcanic province that occupies a zone 900 km long which stretches from eastern Turkey through Soviet Armenia into NE Iran (Fig. 1). The province attains its maximum width of 350 km in the study area where it extends in a SW – NE direction from the Arabian foreland to the Kars Plateau on the Soviet border. The large volume of young volcanic rocks makes Eastern Anatolia one of the few places in the world where it is possible to study variations in lava composition more or less continuously across most of the width of an active continent – continent collision zone.

The aim of this study is to present new geochemical, isotopic and isotopic age data for the Neogene Collision volcanics of Eastern Anatolia, extending work carried out by Lambert et al. (1974), Innocenti et al. (1976, 1980, 1982a, b), and Yilmaz et al. (1987), and to use the results to re-examine the nature and cause of compositional variations in space and time within the province. Having first placed the volcanism into its neotectonic and regional geological framework, we describe the volcanology and petrology of the areas sampled, then examine in turn the major element, trace element and isotopic characteristics of the rocks analysed, and finally consider the petrogenesis and tectonic significance of the data.

Geological setting of the volcanic rocks

Neotectonics of the Eastern Anatolian Collision Zone

The Eastern Anatolian Collision Zone (EACZ) is characterised at present by a plateau at an elevation of about 2 – 2.5 km above sea level, a reflection of thick (c. 50 km) continental crust, and diffuse, shallow seismicity which is indicative of active deformation. Tectonic escape of most of Anatolia is taking place to the west by right-lateral strike-slip along the North Anatolian Fault (NAF) combined with left-lateral strike-slip along the East Anatolian Fault (EAF) (Nowroozi, 1972; McKenzie, 1972; Rotstein and Kafka, 1982; Jackson and McKenzie, 1984; Fig. 1). Current rates of slip are about 0.9 cm a^{-1} for the NAF and 0.2 cm a^{-1} for the EAF; these rates combine to give a westward escape rate for the Anatolian plate of 0.5 cm a^{-1}. The NAF and EAF (McKenzie, 1976) have been active since the mid – late Miocene (Ambraseys, 1970; Tatar, 1975; Ketin, 1976) and show a well-developed surface expression up to 1 km wide, with associated pull-apart basins (Hempton, 1982; Hempton and Dewey, 1983). Tectonic escape along these faults cannot remove much of the strain induced by the Arabian convergence of 1.4 cm a^{-1} (Dewey et al., 1986) and other processes must therefore be active in accommodating the crustal shortening, such as crustal thickening or diffuse, distributed strike-slip faulting (Saroglu et al., 1980; Yilmaz et al., 1987).

The EACZ region is cut by a complex of faults (Fig. 1) which are either SE-trending with a dominantly right-lateral, strike-slip displacement (e.g., Varto Fault, Caldiran Fault, Balik Gölu Fault) or NE- to NNE-trending with dominantly left-lateral, strike-slip displacement (e.g., Malazgirt Fault, Kagizman Fault). Faults of either set may have subordinate vertical displacements, often with a thrust sense (e.g., the Varto fault: Tchalenko, 1977). Some E – W trending faults with a mainly thrust displacement have also been recognised, in particular the fault bounding the northern margin of the Mus Basin, and its continuation into Lake Van. There is relatively minor folding of post middle Miocene strata north of the Bitlis Thrust Zone, presumably associated with ramp structures on thrusts. In general, however, there is no coherent network of linked faults and folds north of the Bitlis Thrust Zone and no obvious direct link between the North Anatolian Fault and the Main Recent Fault of

the Zagros (Tchalenko, 1977).

Normal faults and fissures in the EACZ are minor features compared with the other faults. N – S fissures control the morphology of the Karacalidag volcano on the Arabian foreland and fed the youngest, post-caldera eruptions of Nemrut, implying minimal E – W extension in the foreland and the southern margin of the EACZ. Two other volcanic edifices with N – S elongation can be seen to the east of Cildir Gölu on the northern margin of the Kars Plateau (Fig. 1), perhaps also indicating minor extension in this region. The Akcakale Graben, a small rift structure with N – S normal faults, which is located to the SW of Karacalidag, is another indicator of E – W extension, although this rift appears to act, at least in part, as a transfer structure between some of the outer thrusts of the Arabian foreland sedimentary sequence. The only other normal fault-dominated structure in the EACZ is the small Baskale Graben east of Lake Van on the border between Turkey and Iran.

Pre-collisional geology of the Eastern Anatolian Collision Zone

The EACZ is characterized geologically by three terranes separated by suture zones containing mélanges, accretionary complexes and flysch-molasse basins. The southernmost terrane is the para-autochthonous Arabian foreland which is made up of an almost continuous stratigraphic sequence of mainly shelf sediments of early Palaeozoic to Miocene age resting on a Precambrian basement. At its northern margin, termed the Foothills Structural Belt, the sedimentary rocks have experienced foreland-type thrusting and folding. The central terrane is the Bitlis Massif, an allochthonous terrane of Palaeozoic metamorphic rocks, predominantly metasediments (Hall, 1976). The northern terrane is the Pontide belt which comprises a metamorphic basement of Palaeozoic age overlain by Mesozoic shelf sediments which are in turn overlain by volcanosedimentary complexes of late Cretaceous and Eocene age, assumed, on the basis of their calc-alkaline composition and continuous, linear character, to be subduction-related (Peccerillo and Taylor, 1976). The Black Sea is thought to have formed as a marginal basin behind this Pontide arc. The Pontide Terrane experienced folding towards the end of the Eocene (Brinkmann, 1976) and granitoid intrusion from the late Eocene to early Miocene.

Rocks of the Arabian foreland are separated from the Bitlis Massif by a complex imbricated zone, the Bitlis Thrust (or Suture) Zone (Fig. 1), which contains ophiolitic and island arc assemblages of probable late Cretaceous age (Robertson and Aktas, 1984). Mafic lavas overlain by middle Eocene pelagic chalks within this zone show that an oceanic realm existed between Arabia and the Bitlis microcontinent at that time, although the lavas are of transitional geochemical affinity, possibly indicating that they formed part of the crust of a small, extensional basin rather than a major ocean (Robertson and Aktas, 1984). No subduction-related volcanic rocks younger than late Cretaceous have yet been identified within the Bitlis Suture Zone. Neogene strata, mainly the volcanic rocks that are the subject of this paper, obscure the contact between the Bitlis Massif and the Pontide Terrane. The limited exposure that does exist suggests that the pre-Neogene geology of this zone is dominated by an accretionary complex of Eocene or younger age (Sengör and Yilmaz, 1981).

The Pontide terrane is the product of northward subduction from the beginning of the late Cretaceous to the end of the Eocene. It clearly must have accommodated a large part of the convergence between Arabia and Eurasia during the Palaeogene since, as discussed above, there is little evidence for subduction of this age in the Bitlis Thrust Zone. Collision of the Bitlis Massif with the Pontide Terrane to form the Pontide Suture Zone probably took place in the late Eocene, terminating the calc-alkaline volcanism and causing the folding and subse-

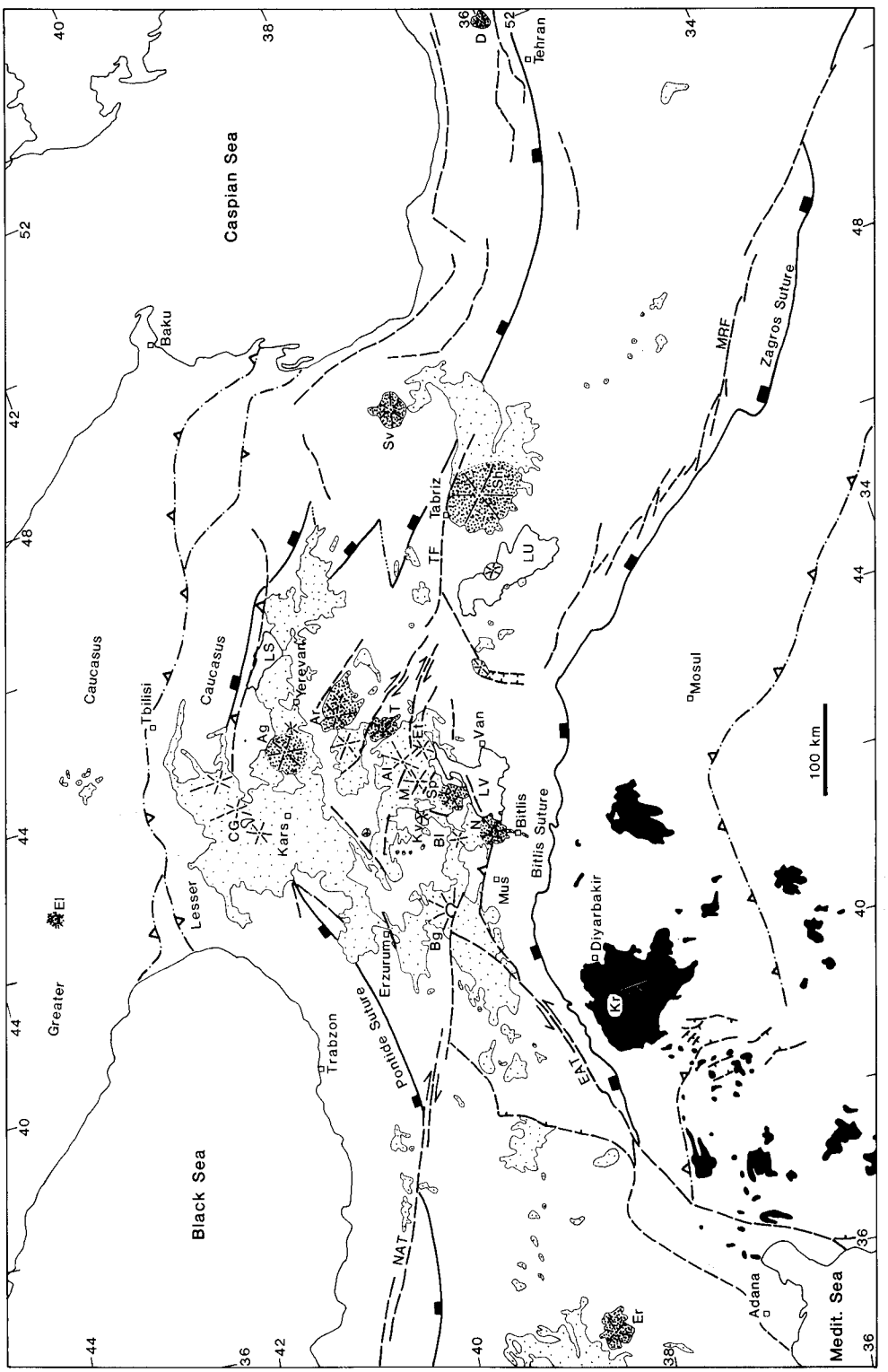

Fig. 1. Distribution and tectonic setting of the late Miocene to Recent volcanics of the Eurasia – Arabia Collision Zone. Black areas = basalts of the Arabian foreland: *Kr* = Karacalidag. Close stipple = young (dormant) volcanoes of the Armenian Plateau: *N* = Nemrut; *Sp* = Süphan; *T* = Tendürek; *Ar* = Ararat (Agri); *Ag* = Aragats (Alagoz); *El* = Elbrus; *Er* = Ercis; *Sh* = Sahand; *Sv* = Savaland; *D* = Demavend. Wider stipple = older (extinct) volcanoes and volcanic strata of the Kars Plateau, Solhan – Mus group and other areas including larger individual volcanic structures: *Bg* = Bingöl; *Kv* = Katavindag; *M* = Meydan; *Et* = Etrusk; *Al* = Aladag. Dashed lines = active faults: with half-arrows = strike-slip; with ticks = normal; with vees = thrust; *NAT* = North Anatolian Transform; *EAT* = East Anatolian Transform; *TF* = Tabriz Fault; *MRF* = Main Recent Fault. Solid lines with black rectangles = Bitlis and Pontide Sutures. Dash-dot line with vees = outer limit of folding and thrusting in the Arabian foreland and in the Koura and Colchide depressions between the Greater and Lesser Caucasus. *LV* = Lake Van; *LU* = Lake Urmiah; *LS* = Lake Sevan; *CG* = Cildir Gölu (lake). Samples in this study were all collected from Turkey, from near Diyarbakir to the north side of Cildir Gölu, covering most of the width of the collision zone.

quent granite plutonism in the Pontide Terrane (Sengör and Yilmaz, 1981).

Timing of the collision event

No consensus has yet been reached about the age of the initial contact between the northern edge of Arabia and the Anatolia – Pontide – Caucasus margin of Eurasia. The minimum proposed age of about 12 Ma (Sengör and Kidd, 1979; Sengör and Yilmaz, 1981) is based on:

(1) The age of the transition from carbonate to flysch/molasse sedimentation seen in the passive margin sedimentary section that is preserved in the thrust belt south of the ophiolites of the BSZ.

(2) The abrupt cessation of marine sedimentation throughout Eastern Anatolia at this time.

(3) The cessation at this time of subduction-related calc-alkaline volcanism and plutonism in the Karkas – Jebel-e-Barez region of the Zagros to the east.

The maximum proposed age of late Eocene (Robertson and Aktas, 1984; Michard et al., 1984) marks the end of subduction-related calc-alkaline volcanism in Eastern Anatolia, both in the Pontide volcanic province in the north and in the volcanic sequences within the BTZ in the south. It is generally agreed that an earlier, late Cretaceous ophiolite emplacement event seen in the foreland thrust belt south of the Bitlis Thrust Zone (Hall, 1976), in the Southern Zagros (Hallam, 1976) and Oman (Gealy, 1977) does not require that the Arabia-Eurasia collision took place at that time, although it does require collision between the Arabian margin and an ophiolitic forearc. The resumption of carbonate-dominated sedimentation over the ophiolitic melange in the Arabian foreland south of the Bitlis Suture shows that the passive margin was essentialy re-established during the Paleogene prior to the main collision event.

A further constraint on the age of initiation of the collision can also be obtained from the amount of convergence (identation) since collision. An estimate, made on the basis of the degree of crustal tickening (taken as 50%) multiplied by the width of the collision zone, yields a value of 250 – 300 km. This estimate does not take into account tectonic escape which is assumed, from the limited total offset on the North Anatolian Fault (about 85 ± 5 km: see references in Sengör and Kidd, 1979), to make only a small contribution to the accommodation of the convergence. A similar value for the convergence is obtained by "matching" the Cretaceous ophiolites of the foreland margin with the possible equivalent complexes in the Troodos – Hatay – Baër Bassit region of the Eastern Mediterranean that have experienced the late Cretaceous, but not the Neogene, emplacement event. At current convergence rates in the direction of maximum shortening (of about 1.5 cm a^{-1}) (Dewey et al., 1986), collision would have to have started about 20 Ma ago.

The discepancies in the estimates for the age of initiation of collision as outlined above are not easy to reconcile. While it is a common consequence of collision for turbiditic clastics to be deposited in a basin floored by the flexurally-loaded continental lithosphere of the impinging passive margin, it is difficult to envisage how, at a yearly convergence rate of 1 cm or more, the initiation of crustal thickening could have been much older than the change from shallow water marine to orogenic clastic sedimentation (commonly with flysch at the base) that is observed in the oldest thrust sheets nearest to the suture. It is possible, however, that the continents had made, or almost made, contact at the end of the Eocene and that Eastern Anatolia in the Oligocene and early Miocene was marked by low-angle subduction that generated little or no arc volcanism, while steeper subduction along the same margin in Iran continued to generate calc-alkaline magmatism into the Miocene. A possible analogue may be the current configuration of the convergent plate margins of the Eastern Mediterra-

nean, where subduction volcanism is taking place in the Aegean but not in Western Turkey.

The volcanic rocks discussed in this paper are, with rare exceptions, no older than 6 Ma. It is clear that they have been generated by processes unconnected with subduction because, at convergence rates of 1.5 cm a^{-1}, an oceanic slab would have sunk below the depths at which arc magmas are generated, even if collision had begun at the latest possible age of 12 Ma.

Evolution of collision-related volcanism

Figure 1 shows the distribution of assumed collision volcanism in Eastern Anatolia and the location of the main sample areas of Karacalidag, the Mus basin, Nemrut, Süphan, Bingöl, Tendürek, Ararat and the Kars Plateau.

In the southern part of the area, on the Arabian foreland, post-Pliocene volcanism has formed the complex basaltic shield of Karacalidag. This volcano is fed by N – S trending fissures (Sengör, 1976) parallel to the nearby Akcakale Graben (Fig. 1).

The central part of the area, between the latitudes of Erzurum and the southern edge of Lake Van, may contain the earliest collision volcanism. Yilmaz et al. (1987) proposed a stratigraphic age of ?middle to late Miocene for the initiation of volcanism in the Solhan – Mus district southwest of Erzurum, and Innocenti et al. (1976) suggested that volcanism began in the Upper Burdigalian (early Miocene). However, apart from one isolated early – middle Miocene isotopic date (13.1 Ma) published by Innocenti et al. (1976) from a lava near the Iranian border, the oldest set of isotopic ages (8.3 – 6.0 Ma) has been obtained by Innocenti et al. (1982b) from the Çat area south of Erzurum. The age of initiation of volcanism thus still requires confirmation. Innocenti et al. (1976) proposed that an initial calc-alkaline phase of volcanism related to northward subduction took place before about 6 Ma, forming a broad volcanic belt parallel to the Bitlis Thrust Zone. According to their model, continued volcanism in the same area gave more alkaline volcanic rocks with ages of 6 – 0 Ma in response to extensional tectonics. This concept of an early subduction-related calc-alkaline event is, however, by no means a consensus view (e.g. Sengör and Kidd, 1979).

The north of the area is dominated by the Kars Plateau, which covers an area of approximately 5000 km^2 with an average elevation of about 1.5 km. The volcanic sequence has been described by Innocenti et al. (1982b) as comprising lava flows with subordinate ignimbrite units and intercalated sediments giving ages from 6.9 ± 0.9 to 1.3 ± 0.3 Ma and comprising an "early Aras lower sequence" (c. 7 – 4 Ma), followed by a "Plateau Sequence" (c. 4 – 2 Ma) and finally by scoriaceous spatter cones of Pleistocene age. Most of the plateau overlies shallow-water sediments of Oligocene age which in turn probably overlie the Pontide Terrane over most of its area.

Volcanic petrology

A set of 107 volcanic samples were collected during three field seasons. The samples form a comprehensive selection of the collision volcanics of the EACZ, predominantly from the volcanoes of Karacalidag, Nemrut, Süphan, Tendürek, Bingöl and Ararat, and the volcanic areas of the Kars Plateau and the Mus Depression, with a small sample set from Bilican, Etrusk and Aladag (Fig. 1). Precise sample locations are available on request. Here we systematically describe the petrology, petrography and volcanic facies for each of the main volcanic regions following the transect from southwest to northeast.

Karacalidag

Karacalidag (1957 m) is a low shield volcano situated on the Arabian foreland, 150 km southwest of the main frontal thrust. The vol-

canic products are predominantly basaltic, erupted since the Pliocene along a N – S trending set of fissures and craters, spatially associated with the nearby Akcakale graben (Fig. 1). Dates between 1.45 Ma and 1.04 Ma have been reported for lavas from the east of the volcano (Sanver, 1968), and similar dates of 0.94 ± 0.33 Ma and 0.83 ± 0.88 Ma were obtained for this paper on lavas from the northern margin of the volcanic complex at Diyarbakir (Table 1). Landsat imagery suggests that some flows, particularly those on the eastern flank, are likely to be much younger, perhaps only a few thousand years old. The samples were collected in a traverse across the shield from 20 km southwest of Siverek to the northern margin at Diyarbakir. The basalts are porphyritic, fine-grained and commonly vesicular, containing phenocrysts of olivine, titanaugite and labradorite in a microcrystalline or fine-grained equigranular matrix. Few evolved rocks are present in the sequence.

Nemrut

Nemrut Dag (3050 m) is a polygenetic stratovolcano that has experienced at least one major episode of caldera collapse, with subsequent rhyolite dome formation and extrusion of trachyandesite onto the caldera floor. On the caldera flanks, small subsidiary domes and cones form a NW – SE trending chain puncturing voluminous air-fall deposits. Mild fumerolic activity is still present on the northwest flank and in the caldera, where there are also hot pools. Nemrut is the only volcano in this region to have a historically-recorded eruption – in 1441 AD (Tchalenko, 1977). Samples 2361 and 2362 come from rhyolite and basalt flows erupted from a N – S fissure on the north flank of the volcano during this event. Sample 2362 gave a K – Ar age of 1.18 ± 0.23 Ma (Table 1), presumably due to excess Ar. A fresh basaltic andesite from the eastern rim of the caldera (Sample 2313) had a very

TABLE 1

Whole-rock K – Ar ages for selected lavas from Eastern Anatolia

Sample	Volcano	SiO_2 (wt.%)	K_2O (wt.%)	Radiogenic ^{40}Ar ($\times 10^{-4}$ mm^3 g^{-1})*	% atmos **	Age (Ma) ± 1 σ
1912	Karacalidag	50.2	1.00	0.303	98.5	0.94 ± 0.33
1913	Karacalidag	48.8	0.90	0.24	99.2	0.83 ± 0.88
2362	Nemrut	47.7	0.68	0.258	96.0	1.18 ± 0.23
2313	Nemrut	64.2	5.12	≤ 1.1	100.0	< 0.7
2112	Mus	50.1	1.32	2.83	97.3	6.0 ± 1.0
2113	Mus	47.5	1.00	1.42	96.5	4.4 ± 0.8
2213	Bingöl	55.4	2.04	2.35	97.9	3.6 ± 0.6
2211	Bingöl	71.1	4.32	4.32	92.1	2.6 ± 0.2
2521	Süphan	62.8	2.71	0.32	99.0	0.36 ± 0.15
2531	Süphan	63.9	2.58	0.19	99.5	0.23 ± 0.19
3132	Ararat	51.4	0.86	0.420	93.3	1.51 ± 0.19

$\lambda_e = 0.581 \times 10^{-10}$ a^{-1}
$\lambda_\beta = 4.962 \times 10^{-10}$ a^{-1}
$^{40}K/K = 1.167 \pm 10^{-2}$ atom%
* Inverse variance weighted mean of two analyses.
** Higher of two measured atmospheric contamination values.

high atmospheric Ar content indicative of a very young age, probably less than 7×10^5 a (Table 1), and one other flow has been dated as Pleistocene (Sanver, 1968).

Samples for analysis were collected from Bitlis, the northern and eastern flanks of the volcano and from the caldera sides and floor. The basalts are vesicular and porphyritic with phenocrysts of plagioclase (labradorite), clinopyroxene and olivine in a fine-grained groundmass containing abundant plagioclase feldspar and magnetite. Trachytes contain polycrystals of andesine and zoned clinopyroxene and occasional resorbed sanidine. The rhyolites have phenocrysts of sanidine and rare clinopyroxene in a holohyaline groundmass.

Mus

The Mus Depression is an E – W trending basin (including the Solhan Group described by Yilmaz et al., 1987), thought to contain volcanics erupted during the early stages of evolution of the province. The volcanics and intercalated sediments form a sequence > 1000 m thick that is dominated by lavas at the base and by pyroclastic deposits in the upper part. The samples were collected from road cuts between Mus and Solhan and in the gorge of the Murat river at the southwest corner of the Mus Basin. We dated two basalt samples from Solhan as 6.0 ± 1.0 Ma and 4.4 ± 0.8 Ma (Table 1). The early lavas are vesicular basalts and basaltic andesites with phenocrysts and glomerocrysts of clinopyroxene and olivine and large, slightly zoned bytownite – labradorite in a groundmass of plagioclase and clinopyroxene with accessory magnetite and variolitic glass.

Bingöl

Bingöl Daglari (3250 m) forms a half caldera cut by the Varto Fault, a continuation of the Northern Anatolian Fault, and is predominantly composed of basaltic andesites and rhyolites. The samples were collected from the southern and eastern margins of the Bingöl Caldera between Hinis, Varto and Caylar. A basaltic andesite and a later stage rhyolite gave ages of 3.6 ± 0.6 Ma and 2.6 ± 0.2 Ma, respectively (Table 1). The basaltic andesites have phenocrysts of clinopyroxene and large, zoned plagioclase (labradorite – andesine) in a groundmass dominated by plagioclase and minor clinopyroxene with interstitial magnetite. The rhyolites have phenocrysts of sanidine, zoned albite and biotite in a cryptocrystalline groudmass.

Süphan

Süphan Dagi (4434 m) is a polygenetic stratovolcano made up of a complex of numerous eruptive domes and cones with intercalated lava flows and pyroclastics. Samples were collected from the southern and eastern margins from Adilcevas to Sarusu. The lavas range in composition from basalt to rhyolite but are predominantly intermediate. Dates published by Innocenti et al. (1976) show Süphan to have been active from at least 0.7 Ma to 0.4 Ma and to rest locally on a 5.8 Ma volcanic basement. Two andesites dated for this study gave slightly younger K – Ar ages of 0.36 ± 0.15 Ma and 0.23 ± 0.19 Ma (Table 1). The late-stage domes rest on these lavas and must thus be younger than the latter age. The domes form a complex radiating pattern around the main crater. The intermediate volcanics are commonly vesicular and contain phenocrysts of zoned plagioclase, sanidine, hypersthene and clinopyroxene with rare hornblende in a fine-grained groundmass of plagioclase, pyroxene and interstitial magnetite. The rhyolites contain phenocrysts of zoned sodic plagioclase, K feldspar and biotite in a cryptocrystalline groundmass.

Tendürek

Tendürek (3584 m) is a polygenetic volcano, built by small fissure eruptions followed by central eruptions and caldera collapse. The caldera collapse led to late-stage volcanic activity, which included an episode of basalt eruption and subsequent development of parasitic cones. The oldest age determination is 2.5 Ma (Innocenti et al., 1976) and recent fumarolic activity has been recorded along the Caldiran Fault (Sanver, 1968). The samples were collected across the volcano from Kizildiz in the north to Caldiran in the south. The lithologies are predominantly basalts and trachyandesites. The basic lavas contain phenocrysts of plagioclase and clinopyroxene and rare olivine and opaques in a plagioclase-rich groundmass; the intermediate lavas contain large zoned plagioclase (oligoclase – andesine) and glomerocrysts of clinopyroxene and magnetite, also in a plagioclase-rich groundmass.

Ararat

Ararat (Agri Dag) forms a polygenetic double-peaked (5165 m and 3903 m) stratovolcano, covering an area of about 1000 km^2 and sitting, according to Dewey et al. (1986), in a complex, sinistral pull-apart basin. Samples were collected from the southern and western margins of the volcano, from Dogubayazit to Igdir and east of Dogubayazit towards the Iranian border. Ararat is predominantly composed of basic and intermediate lavas with supplimentary pyroclastic products and rhyolites. The final products were erupted from a NW – SE aligned series of parasitic cones dated at 0.5 Ma (Sanver, 1968). An early basalt, dated as part of this study, gave an age of 1.51 ± 0.19 Ma (Table 1). The basalts are porphyritic with zoned plagioclase and clinopyroxene and occasional olivine phenocrysts in a fine-grained, holocrystalline, vesicular groundmass consisting of plagioclase, clinopyroxene and opaques. The porphyritic andesites show zoned andesine with corroded cores and glomerocrysts of clinopyroxene, orthopyroxene and opaques with rare hornblende "ghosts" in a fine-grained or cryptocrystalline groundmass. The dacites contain oligoclase and clusters of clinopyroxene in a cryptocrystalline groundmass, while the rhyolites contain zoned oligoclase and biotite phenocrysts in a fine-grained matrix of biotite, feldspar and quartz.

Kars

The Kars Plateau samples were collected from a number of sites on a transect from Kagizman in the south to Cildir Gölu and Ardahan in the north, where a good stratigraphic section through the (about 7 – 1.5 Ma) volcanic pile is exposed. Samples were also collected from localities near Sarikamis and Oltu. The lavas are predominantly basic and intermediate. The basalts are porphyritic, rarely vesicular, with phenocrysts of plagioclase (up to 50%) and subordinate clinopyroxene, olivine and orthopyroxene in a fine-grained groundmass. The intermediate rocks have an occasionally vesicular, microcrystalline to cryptocrystalline matrix with disseminated phenocrysts commonly forming glomerocrysts of plagioclase, clinopyroxene and orthopyroxene and magnetite. The plagioclase phenocrysts are typically labradorite – oligoclase in composition and zoned with cores exhibiting reaction rims. Ignimbrite deposits, common at the base of the sequence, typically contain pyrogenic crystals of plagioclase, K feldspar and pyroxenes.

Analytical techniques

A total of 105 samples from Eastern Anatolia were powdered using an agate ball mill. Of these, 27 samples were analysed for major elements by electron microprobe on fused glasses at SUNY Stony Brook (Bender et al., 1984) and the trace elements Zr, Nb, Sr, Rb, Ni, Zn, Cr and V, at the University of

TABLE 2

Major element and XRF trace element data from the Eastern Anatolia Collision Zone used in this paper

Volcano:	KARA	KARA	KARA	KARA	KARA	KARA	KARA	KARA	KARA	KARA	BTLC
Sample no:	PL67	PL2/5	PL2/4	PL2/1	PL2/2	PL2/3	1911	1913	1912	PL66	2031
Rock type:	Bas	Bas	Bas	Bas	Bas	Bas	Bas	Bas	Bas	Bas	Bas
wt.%:											
SiO_2	45.40	45.60	46.00	46.10	46.30	47.30	46.70	48.80	50.20	46.90	46.40
TiO_2	2.88	3.44	2.88	2.04	1.84	2.83	2.50	2.39	2.62	2.46	3.39
Al_2O_3	14.44	13.36	15.42	13.92	15.16	15.48	13.80	14.40	15.10	13.24	16.90
Fe_2O_3	14.40	14.36	14.08	12.28	12.56	13.66	14.40	13.50	12.98	13.20	14.50
MnO	0.18	0.18	0.17	0.15	0.16	0.17	0.17	0.16	0.16	0.16	0.19
MgO	8.90	9.38	5.64	7.60	6.38	5.70	9.51	9.92	7.66	9.24	5.31
CaO	9.10	8.60	10.70	11.94	10.28	9.68	8.76	8.20	8.88	8.44	7.59
Na_2O	3.66	3.14	3.10	2.84	3.00	3.34	2.62	2.52	3.28	3.64	3.99
K_2O	1.44	1.44	0.78	0.78	0.68	1.02	0.95	0.90	1.00	0.88	1.05
P_2O_5	0.51	0.61	0.47	0.32	0.30	0.46	0.34	0.26	0.26	0.30	0.52
LOI	−0.12	0.46	0.92	2.41	1.54	0.09	0.26	0.80	−0.47	1.31	0.39
Total	100.79	100.57	100.16	100.38	98.20	99.73	100.01	101.85	101.67	99.77	100.23
ppm:											
Rb	17	13	8	11	8	10	13	15	12	9	11
Sr	827	735	660	360	409	592	544	584	514	647	614
Ba	165		104		141	158	159	134	137	103	
Zr	217	259	171	111	131	160	154	141	151	154	322
Y	20	21	20	15	20	20		18	21	18	
Nb	40	37	22	15	14	25	26	18	23	23	18
Th		7	4	6	7	5	2	4	4	3	
Pb	2	2	n.d	n.d	1	2		1	1	1	
Sc	23							24	28	25	
Cr	280	320	147	440	340	78	286	420	300	320	11
V	249	244	326		234		176	243	275	248	163
Ni	193	242	77	155	80	66	244	239	161	226	35
Co	53	57	46	52	48	45		56	45	53	
Cu	74	62	67	122	56	60		45	50	86	
Zn	140	138	120	105	109	117	98	126	125	126	90
Analysis	NX,NA	NX,NA,D	NX,NA	NX,NA,D	NX,NA,D	NX,NA,D	M,O	NX,NA	NX,NA	NX,NA	M,O

TABLE 2 (continued)

Volcano:	MUS	MUS	MUS	MUS	MUS	MUS	MUS	MUS	MUS	MUS	NEM
Sample no:	2113	2112	2115	2114	2121	2111	PL2/32	2141	PL2/31	2142	2362
Rock type:	Bas	TrBas	TrAnd	TrAnd	TrAnd	TrAnd	TrAnd	Trac	Rhy	Rhy	Bas
wt.%:											
SiO_2	47.50	50.10	51.20	52.00	53.00	53.70	56.10	66.20	70.10	74.00	47.70
TiO_2	2.84	2.86	2.98	3.33	2.21	1.45	1.47	0.50	0.47	0.05	3.08
Al_2O_3	16.50	15.56	15.36	16.30	16.90	18.20	17.04	18.00	15.28	13.70	16.66
Fe_2O_3	12.42	12.60	12.74	11.50	10.80	9.53	8.90	2.54	3.12	1.42	14.10
MnO	0.18	0.20	0.15	0.21	0.21	0.18	0.11	0.00	0.02	0.05	0.20
MgO	5.92	4.60	1.02	1.88	1.84	2.21	1.74	0.00	0.22	0.00	6.46
CaO	8.56	8.00	5.84	7.68	6.87	6.38	5.58	2.01	2.02	0.39	9.48
Na_2O	2.86	3.92	4.40	4.36	4.92	4.90	4.58	5.52	4.24	5.06	3.54
K_2O	1.00	1.32	2.40	2.00	2.64	2.21	2.04	4.32	3.84	4.37	0.68
P_2O_5	0.44	0.49	1.48	0.83	0.82	0.44	0.85	0.19	0.02	0.01	0.37
LOI	2.60	1.24	3.39	1.54	2.93	1.68	1.04	1.11	0.90	0.57	−0.02
total	100.82	100.89	100.96	101.63	103.14	100.88	99.45	100.39	100.23	99.62	102.25
ppm:											
Rb	22	28	68	57	79	63	61	138	140	176	7
Sr	397	393	483	375	389	422	443	242	178	1	401
Ba	153	180	361	268		184	536	409			125
Zr	211	313	397	431	646	430	358	647	237	281	200
Y	31	39	56	56	61	40	37	56	22	67	31
Nb	13	21	35	31	32	28	31	39	20	79	11
Th	3	3	7	8	12	13	16	21	26	24	2
Pb	8	6	16	10	13	7	9	20	24	30	0
Sc	31	26	13	19							24
Cr	71	99	13	41	6	12	9	n.d.	12	8	97
V	285	253	100	158	52	67	104	n.d.	51	2	250
Ni	39	23	8	6	11	21	2	11	4	7	44
Co	36	30	13	21			17		3		44
Cu	55	40	25	46			14		5		40
Zn	113	127	142	144	118	100	110	83	56	110	116
Analysis	NX,NA	NX,NA	NX,NA	NX,NA	M,O,NX	M,O,NX,D	NX,NA,D	M,O,NX	NX,NA	M,O,NX	NX,NA

TABLE 2 (continued)

Volcano:	NEM	NEM	NEM	NEM	NEM	NEM	NEM	NEM	NEM	NEM	NEM
Sample no:	2411	PL52	PL55	PL54	PL63	PL51	PL56	2022	2313	2421	PL50
Rock type:	TrBas	Bas	TrAnd	TrAnd	TrAnd	Trac	Trac	Trac	Trac	Trac	Rhy
wt.%:											
SiO_2	48.50	48.90	52.90	52.70	58.00	62.60	64.20	64.30	64.20	66.00	71.30
TiO_2	3.12	2.00	2.60	2.44	1.38	0.52	0.58	0.55	0.48	0.42	0.43
Al_2O_3	15.80	16.60	16.34	16.30	15.78	17.46	17.44	15.70	15.30	16.20	10.28
Fe_2O_3	13.60	12.68	10.54	10.60	9.36	4.08	4.76	5.54	6.49	4.35	7.14
MnO	0.24	0.18	0.21	0.21	0.16	0.11	0.13	0.19	0.23	0.12	0.18
MgO	3.59	6.00	3.42	3.44	2.12	0.56	0.38	0.26	0.00	0.00	0.06
CaO	7.43	9.02	7.26	7.42	5.24	1.98	2.54	1.41	1.51	1.20	0.44
Na_2O	4.22	3.16	4.86	4.54	4.16	6.40	6.04	6.02	6.15	6.14	6.12
K_2O	2.20	1.40	2.32	2.44	2.54	4.56	4.24	5.58	5.12	4.81	4.56
P_2O_5	1.24	0.36	0.86	0.91	0.51	0.13	0.13	0.10	0.07	0.07	0.02
LOI	−0.13	0.81	0.00	0.37	0.26	0.47	0.08	0.42	0.58	0.37	0.30
Total	99.81	101.11	101.31	101.37	99.51	98.87	100.52	100.07	100.13	99.68	100.83
ppm:											
Rb	59	35	63	66	90	101	81	93	87	98	190
Sr	510	456	575	566	237	168	172	19	29	94	3
Ba				470	428	1094	905	245			806
Zr	395	232	340	338	366	356	372	466	453	531	1425
Y		30	48	46	51	34	39			51	136
Nb	25	14	26	25	21	25	24	33	30	34	76
Th		6	7	7	12	8	9	9		12	33
Pb		3	8	8	15	11	10			11	33
Sc		21	15	18	21	5	5				4
Cr	2	29	21	24	74	19	40	1	n.d.	8	40
V	69	261	111	198	149	30	39	n.d.	3	n.d.	21
Ni	5	33	7	7	9	7	4	9	10	n.d.	6
Co		45	22	21	18	n.d.	n.d.				n.d.
Cu		33	14	17	21	9	10				10
Zn	119	112	121	110	115	73	82	103	112	53	219
Analysis	M,O	NX,NA	NX,NA	NX,NA	NX,NA	NX,NA	NX,NA	M,O	M,O	M,O	M,O

TABLE 2 (continued)

Volcano:	NEM	NEM	NEM	NEM	NEM	NEM	SUP	SUP	SUP	SUP	SUP
Sample no:	2351	2321	PL53	PL57	PL65	PL59	PL2/8	PL68	PL70	PL74	PL71
Rock type:	Rhy	Rhy	Rhy	Rhy	Rhy	Rhy	TrBas	TrAnd	TrAnd	TrAnd	TrAnd
wt.%:											
SiO_2	72.40	74.20	74.50	74.90	75.00	75.40	49.00	51.50	51.50	54.90	55.70
TiO_2	0.21	0.13	0.21	0.24	0.11	0.09	3.43	2.08	1.71	1.91	1.81
Al_2O_3	12.50	12.80	12.80	10.24	12.48	12.98	15.32	17.90	18.44	16.04	15.56
Fe_2O_3	3.57	2.20	3.38	4.94	2.30	2.08	13.50	11.20	10.34	11.06	10.98
MnO	0.06	0.04	0.08	0.11	0.05	0.05	0.24	0.21	0.18	0.18	0.18
MgO	0.00	0.00	0.04	0.08	0.02	0.04	3.78	4.20	3.80	3.14	2.81
CaO	0.33	0.27	0.42	0.32	0.34	0.34	7.58	6.70	7.64	6.68	5.84
Na_2O	5.45	5.08	5.28	5.28	4.80	4.80	4.04	4.96	4.98	3.68	3.62
K_2O	4.65	4.65	4.80	4.40	4.48	4.60	2.20	1.58	1.84	2.00	2.16
P_2O_5	0.00	0.01	0.13	0.01	0.01	0.02	1.37	0.99	0.77	0.37	0.40
LOI	0.69	0.76	0.22	0.47	0.00	0.00	−0.04	0.34	−0.18	0.48	1.66
Total	99.86	100.14	101.86	100.99	99.59	100.40	100.42	101.66	101.02	100.44	100.72
ppm:											
Rb	200	201	291	186	177	169	53	22	35	62	69
Sr	1	1	3	2	1	3	584	676	619	250	239
Ba			19	15	1	440	482	438	468	321	414
Zr	1321	748	1247	1272	722	609	381	393	358	356	287
Y	115	105	129	126	105	96	55	43	38	45	36
Nb	70	64	84	67	63	56	31	36	29	37	16
Th	37	31	32	31	30	27	10		10	8	10
Pb	31	27	32	31	26	26	4	39	48	13	9
Sc			1	4	4	4		16	13	26	24
Cr	n.d.	2	46	56	51	41	5	28	18	16	19
V	1	1	18	21	5	34	166	163	130	293	304
Ni	9	7	6	4	7	4	7	6	9	9	9
Co			n.d.	n.d.	n.d.	n.d.	25	20	17	23	22
Cu			10	7	6	5	10	17	18	17	16
Zn	172	125	144	192	119	105	147	134	142	121	121
Analysis	NX,NA	NX,NA	NX,NA	NX,NA	NX,NA	NX,NA	NX,NA,D	NX,NA	NX,NA	NX,NA	NX,NA

TABLE 2 (continued)

Volcano:	SUP	SUP	SUP	SUP	SUP	SUP	SUP	SUP	BIN	BIN	BIN
Sample no:	PL73	PL69	PL2/9	2521	2531	PL2/7	2541	PL72	2213	2212	2214
Rock type:	TrAnd	TrAnd	TrAnd	Trac	Trac	Trac	Rhy	Rhy	TrAnd	TrAnd	Rhy
wt.%:											
SiO_2	56.00	56.80	57.70	62.80	63.90	66.30	73.10	75.20	55.40	58.20	70.60
TiO_2	1.88	1.89	1.54	1.01	0.87	0.72	0.21	0.00	1.28	1.34	0.36
Al_2O_3	16.04	16.32	15.92	16.10	17.30	15.52	14.20	13.66	17.98	17.90	15.30
Fe_2O_3	10.54	10.90	8.64	6.38	5.90	4.38	1.76	1.24	7.36	7.69	2.30
MnO	0.18	0.18	0.14	0.11	0.11	0.08	0.05	0.05	0.16	0.17	0.04
MgO	3.04	3.02	2.70	1.45	1.33	1.14	0.16	0.04	1.72	1.37	0.24
CaO	6.70	6.20	5.64	3.94	3.80	3.08	1.41	0.57	7.20	5.94	1.56
Na_2O	3.76	3.80	4.17	4.79	5.71	4.64	4.08	3.86	4.26	4.32	4.22
K_2O	2.16	2.16	1.86	2.71	2.58	3.02	4.31	4.62	2.04	2.36	4.84
P_2O_5	0.37	0.39	0.26	0.32	0.24	0.19	0.06	0.03	0.31	0.32	0.11
LOI	0.18	−0.18	1.07	1.05	0.46	1.73	1.70	1.41	2.52	2.12	1.89
Total	100.85	101.48	99.64	100.65	102.20	100.80	101.04	100.68	100.23	101.73	101.46
ppm:											
Rb	72	74	57	82	80	89	112	160	68	75	155
Sr	245	249	253	207	200	155	96	6	460	433	155
Ba	405		351		392	388		51	135		
Zr	224	333	241	364	338	349	154	86	254	306	307
Y	43	46	36	45		37		31	23		19
Nb	15	18	13	13	10	10	27	6	18	20	23
Th	11	10	12	10		13		19	8		22
Pb	11	26	8	12		14		25	12		21
Sc	23	26						5			
Cr	19	22	12	3	6	8	2	59		24	2
V	298	311	177	46	42	70	12	23		108	13
Ni	9	9	9	6	10	9	7	4		33	6
Co	25	23	22			6		n.d.			
Cu	16	15	13			9		6			
Zn	120	118	98	76	70	68	50	40		73	41
Analysis	NA,NX	NA,NX	NX,NA,D	M,O,NX	M,O	NX,NA,D	M	NX,NA	NX	M,O	M,O,NX

TABLE 2 (continued)

Volcano:	BIN	ETR	ALA	ALA	TEN	TEN	TEN	TEN	TEN	TEN	TEN
Sample no:	2211	2512	3211	3221	PL82	3121	PL75	PL76	PL81	PL79	PL80
Rock type:	Rhy	Trac	Trac	Trac	TepPho	Trbas	Bas	Bas	TrAnd	TrAnd	TrAnd
wt.%:											
SiO_2	71.10	66.90	66.90	67.20	48.30	48.90	49.10	50.10	51.40	52.90	56.00
TiO_2	0.35	0.70	0.68	0.62	2.37	2.35	1.98	1.94	2.54	1.72	2.30
Al_2O_3	14.90	16.40	16.20	16.30	18.40	17.00	16.94	16.42	17.48	17.76	16.24
Fe_2O_3	2.12	2.83	3.13	2.81	11.96	11.70	11.54	11.42	11.14	10.08	10.72
MnO	0.02	0.06	0.09	0.09	0.18	0.20	0.18	0.18	0.21	0.18	0.18
MgO	0.21	0.26	0.39	0.34	3.20	4.10	5.98	5.58	4.28	3.56	3.08
CaO	1.46	1.61	1.53	1.48	7.18	6.53	9.20	6.54	6.52	6.84	6.28
Na_2O	5.41	5.64	4.40	5.55	6.28	5.38	3.90	3.98	4.98	4.88	3.84
K_2O	4.32	4.80	5.35	4.82	2.00	1.56	0.94	0.86	1.62	1.70	2.02
P_2O_5	0.10	0.13	0.16	0.18	0.66	1.02	0.41	0.49	0.89	0.73	0.40
LOI	0.50	0.55	2.83	0.20	0.00	0.24	0.07	3.96	0.02	0.04	0.00
Total	100.49	99.88	101.66	99.59	100.53	98.98	100.24	101.47	101.08	100.39	101.06
ppm:											
Rb	153	155	181	177	42	22	20	18	23	21	74
Sr	145	177	180	191	735	695	404	422	682	641	258
Ba	191				393	329	178	171			319
Zr	293	547	537	601	335	389	246	236	380	341	324
Y	21			50	35	42	36	37	43	37	46
Nb	23	38	45	48	26	34	15	14	35	30	19
Th	24			32	7	6	4	4	6	8	9
Pb	24			28	8	12	8	5	9	11	10
Sc					10		28	26	16	14	24
Cr	9	3	3	3	32	n.d.	49	47	23	12	19
V	14	27	26	22	145	106	256	274	163	161	260
Ni	9	11	5	5	6	12	58	46	9	4	7
Co					27		40	37	20	21	22
Cu					17		40	39	16	17	15
Zn	53	71	71	71	135	114	106	108	130	148	122
Analysis	M,O,NX	M,O	M,O	M,O	NX,NA	M,O,NX	NX,NA	NX,NA	NX,NA	NX,NA	NX,NA

TABLE 2 (continued)

Volcano:	TEN	TEN	ARA	ARA	ARA	ARA	ARA	ARA	ARA	ARA	ARA
Sample no:	PL77	3111	PL83	3132	3071	PL2/11	3031	PL78	3051	3041	PL2/10
Rock type:	TrAnd	TrAnd	TrBas	Bas	And	And	And	And	And	And	And
wt.%:											
SiO_2	57.40	58.40	47.20	51.40	56.00	56.30	56.60	58.50	57.10	58.20	61.60
TiO_2	1.30	1.24	2.44	2.08	1.08	1.54	1.35	0.80	1.11	0.97	0.78
Al_2O_3	17.86	18.10	17.04	17.54	16.80	16.34	16.94	16.22	17.80	17.50	16.20
Fe_2O_3	6.48	5.98	13.76	9.88	7.80	8.46	7.60	5.84	7.21	6.37	5.36
MnO	0.16	0.14	0.19	0.15	0.12	0.15	0.11	0.10	0.11	0.09	0.08
MgO	1.68	1.34	4.70	6.68	5.00	2.50	3.16	4.08	4.01	4.08	3.54
CaO	3.64	3.56	9.22	8.42	8.00	5.76	6.08	7.16	7.21	6.57	5.92
Na_2O	6.52	6.56	4.88	4.12	3.53	4.24	4.28	3.24	3.80	4.22	4.00
K_2O	3.66	3.73	1.48	0.86	1.10	1.92	1.82	2.12	1.52	1.80	1.32
P_2O_5	0.46	0.42	0.54	0.33	0.25	0.38	0.31	0.29	0.33	0.30	0.19
LOI	0.26	0.39	−0.15	0.17	0.33	1.98	0.82	0.13	0.54	0.29	0.69
Total	99.42	99.86	101.30	101.63	100.01	99.57	99.07	98.48	100.74	100.39	99.68
ppm:											
Rb	107	95	28	11	23	45	47	44	37	46	36
Sr	292	286	579	531	378	369	463	471	435	532	388
Ba	553	538	381	221			461				430
Zr	562	475	296	187	165	262	229	174	206	203	184
Y	52	54	36	26		38	28	22	25	22	18
Nb	42	41.7	21	10.1	10.2	18.2	12.1	17	15.2	13.1	12.2
Th	10	13	6	3		8	8	8	7	9	8
Pb	18	17	5	3		6	10	12	6	8	8
Sc	1		18	28			16	20			
Cr	20	11	26	298	54	6	81	120	42	103	79
V	69	36	233	213	141	170	191	148	135	111	106
Ni	6	7	20	100	36	9	25	53	43	67	57
Co	8		35	32		20	19	16			21
Cu	9		18	43		15	26	28			31
Zn	117	114	135	89	84	100	84	78	79	69	66
Analysis	NX,NA	M,O,NX	NX,NA	NX,NA,D	M,O	NX,NA,D	NX,NA	NX,NA	NX,NA	M,O,NX	NX,NX,D

TABLE 2 (continued)

Volcano:	ARA	ARA	ARA	ARA	KARS	KARS	KARS	KARS	KARS	KARS	KARS
Sample no:	3131	PL85	PL84	3062	3011	PL88	PL89	PL87	2821	PL2/22	3021
Rock type:	And	And	Dac	Rhy	Bas	Bas	Bas	TrBas	Bas	TrAnd	BasAnd
wt.%:											
SiO_2	62.60	62.70	63.50	76.50	46.00	47.50	47.90	48.40	50.60	53.20	54.50
TiO_2	0.79	0.86	0.90	0.08	2.42	2.47	2.90	3.05	2.08	1.53	1.18
Al_2O_3	18.00	16.54	16.32	13.80	16.90	17.36	16.76	16.92	17.86	17.56	16.92
Fe_2O_3	5.40	5.32	5.48	1.13	13.90	13.28	13.48	13.64	10.70	7.66	8.20
MnO	0.09	0.09	0.09	0.04	0.21	0.18	0.19	0.19	0.16	0.12	0.12
MgO	1.42	2.32	2.38	0.00	5.81	5.10	5.34	5.34	5.99	3.72	4.88
CaO	4.59	5.56	5.20	0.76	8.49	7.96	7.82	7.68	8.18	7.78	8.14
Na_2O	4.67	4.26	4.24	4.54	4.04	4.00	4.04	4.22	3.85	4.10	3.56
K_2O	1.81	2.06	2.22	3.44	0.61	0.94	0.98	1.02	0.84	1.66	1.48
P_2O_5	0.29	0.25	0.25	0.04	0.58	0.38	0.38	0.40	0.21	0.47	0.28
LOI	0.47	1.20	0.74	0.11	1.13	1.28	0.31	0.14	0.47	0.79	0.46
Total	100.13	101.16	101.32	100.44	100.09	100.45	100.10	101.00	100.94	98.59	99.72
ppm:											
Rb	41	60	63	88	5	12	13	14	12	35	31
Sr	379	392	389	75	518	513	496	497	367	520	426
Ba		528	526	395				244	191	351	
Zr	207	237	243	89	275	199	213	212	147	268	171
Y		24	24			28	32	31	28	28	24
Nb	13	13	13	12	10	11	12	12	7	33	13
Th		7	8	9		5	1	4	4	9	5
Pb		11	9			3	4	3	6	5	6
Sc		8	15			16	15	18	33		20
Cr	5	25	50	2	22	34	53	50	125	51	180
V	56	106	120	3	120	255	251	273	258	176	188
Ni	10	15	18	6	43	29	26	27	61	37	67
Co		18	14			38	36	38	40	26	26
Cu		27	23			22	32	32	37	42	49
Zn	73	72	73	40	89	118	135	122	96	89	83
Analysis:	M,O	NX,NA	NX,NA	M,O	M,O	NX,NA	NX,NA	NX,NA	NX,NA	NX,NA,DX	NX,NA

TABLE 2 (continued)

Volcano:	KARS	KARS	KARS	KARS	KARS	KARS	KARS	KARS	KARS	KARS	KARS
Sample no:	PL2/26	PL2/23	2931	PL2/19	PL2/17	2941	2921	2961	PL2/20	PL2/15	2911
Rock type:	BasAnd	TrAnd	BasAnd	BasAnd	And	And	And	And	And	And	And
wt.%:											
SiO_2	55.00	55.20	55.50	55.80	57.50	59.00	60.20	60.50	60.50	61.70	62.70
TiO_2	1.09	1.85	1.25	1.24	0.81	1.01	0.90	0.87	0.93	0.88	0.79
Al_2O_3	16.58	16.60	17.10	17.12	16.92	16.38	16.30	17.30	16.16	16.58	16.50
Fe_2O_3	7.94	8.88	8.46	8.00	6.78	6.65	5.84	5.90	5.84	4.92	5.51
MnO	0.12	0.14	0.12	0.07	0.12	0.99	0.09	0.09	0.08	0.04	0.08
MgO	4.90	2.64	4.69	2.54	4.52	3.18	2.50	2.94	2.52	2.26	2.52
CaO	8.14	6.86	7.58	7.74	7.72	5.59	5.16	5.87	5.34	5.16	5.08
Na_2O	3.50	4.48	3.92	3.90	3.48	3.82	3.84	4.43	3.40	4.14	3.91
K_2O	1.28	1.84	1.48	1.10	1.22	2.14	2.70	1.46	2.26	1.90	2.28
P_2O_5	0.32	0.38	0.34	0.37	0.18	0.25	0.24	0.25	0.31	0.33	0.21
LOI	0.69	0.66	0.42	1.23	0.68	1.50	1.50	0.33	2.07	0.91	
Total	99.56	99.53	100.86	99.11	99.93	100.51	99.27	99.94	99.41	98.82	99.58
ppm:											
Rb	24	46	30	19	30	60	64	30	45	43	61
Sr	421	450	491	470	427	386	416	503	514	550	346
Ba		403		323	354		461		549	540	
Zr	164	259	198	175	136	222	225	180	197	188	194
Y	22	29		23	18	24	21		17	16	
Nb	12	19	14	12.8	9	15	16	10.6	14	13	13
Th	8	9	5	6	10	8	10	5	12	12	
Pb	6	6		3	5	11	11		6	7	
Sc						20	13				
Cr	118	12	58	212	93	104	59	24	52	96	28
V	252	211	130	185	130	166	119	84	124	127	86
Ni	71	10	57	54	65	47	26	33	35	49	27
Co	28	25		18	31	17	13		17	17	
Cu	40	42		47	30	34	20		30	45	
Zn	84	90	73	75	76	76	67	66	82	67	61
Analysis:	NX,NA,D	NX,NA,D	M	NX,NA,D	NX,NA,D	NX,NA	NX,NA	M,O	NX,NA,D	NX,NA,D	M,O

TABLE 2 (continued)

Volcano:	KARS	KARS	KARS	KARS	KARS	KARS
Sample no:	PL2/21	2971	PL2/18	PL2/13	PL2/14	2811
Rock type:	Dac	Dac	Dac	Dac	Rhy	Rhy
wt.%:						
SiO_2	64.40	65.60	67.50	67.70	72.90	75.50
TiO_2	0.99	0.63	0.44	0.53	0.11	0.09
Al_2O_3	17.12	16.00	16.12	15.62	12.58	13.50
Fe_2O_3	4.64	4.43	3.38	2.98	1.64	0.79
MnO	0.03	0.06	0.04	0.06	0.06	0.04
MgO	0.26	2.46	1.42	0.54	0.06	0.00
CaO	4.66	4.83	3.94	2.64	0.60	0.44
Na_2O	4.60	3.85	3.80	3.92	3.66	3.88
K_2O	1.94	2.15	2.06	3.38	4.60	4.48
P_2O_5	0.35	0.20	0.17	0.24	0.02	0.01
LOI	1.17	1.44	0.97	2.74	2.97	0.64
Total	100.16	101.65	99.84	100.35	99.20	99.37
ppm:						
Rb	50	59	65	80	102	137
Sr	554	449	422	245	11	23
Ba	701		595	631	501	424
Zr	225	183	147	312	230	93
Y	22	17	10	33	55	24
Nb	13	12	12	21	18	14
Th	11	8	13	14	25	
Pb	8	11	6	15	19	
Sc						
Cr	8	66	22	6	5	16
V	126	70	61	45	21	21
Ni	6	40	23	6	4	6
Co	11		10	7	2	
Cu	26		32	3	3	
Zn	73	59	54	81	61	38
Analysis:	NX,NA,D	M,O,NX	NX,NA,D	NX,NA,D	NX,NA,D	M,O,D

KARA = Karacaladag; *MUS* = Mus district; *NEM* = Nemrut; *BIN* = Bingöl; *SUP* = Süphan; *BILC* = Bilican; *ETR* = Etrusk; *ALA* = Aladag; *TEN* = Tendürek; *ARA* = Ararat; *KARS* = Kar Plateau. Rock types: *BAS* = basalt; *BasAnd* = basaltic andesite; *And* = andesite; *Dac* = dacite; *Rhy* = rhyolite; *TrBas* = trachybasalt; *TrAnd* = trachyandesite; *Trac* = trachyte; *TepPho* = tephrophonolite. Sources of data (for analytical details, see text): *M* = Massachusetts; *O* = Oxford; *N* = Newcastle; *D* = Durham, *X* = XRF; *A* = atomic absorption; *n.d.* = not determined.

Massachusetts using a Siemens SRS – 200 XRF spectrometer with a Au tube (Autio and Rhodes, 1983). Eighty samples were analysed at the University of Newcastle upon Tyne for major elements and the trace elements, Ni, Zn, Cr, Co, V, Sc, Cu and Ba, on a Varian AA – 575 atomic absorption spectrometer (AAS). Also at Newcastle, 93 samples were analysed for the trace elements Rb, Sr, Zr, Y, Nb, Th and Pb using a Philips PW 1415 XRF spectrometer with a Rh anode tube (Pearce et al., 1986) and 36 samples were analysed on the same type of spectrometer at Oxford for Rb and Sr. A subset of these samples were also analysed at Durnham University for Zr, Y, Nb, Ba, Th, Pb, Cu, Zn, Cr, Ni and V using a Philips PW 1500 spectrometer with a Rh anode tube. Interlaboratory comparison showed comparability to $< 5\%$, except in two cases where a 5% systematic variation between techniques was identified and the discrepant analyses corrected. When more than one technique has been used to analyse a given sample, the data are presented as averages. The full data set is presented in Table 2. Approximate detection limit concentrations in ppm at the 95% confidence level are: Zr, Sr, Rb, Zn, Cu and Y, 2; Nb, 1; Ni, Th, Sc and Co, 5; Cr, V and Ba, 10.

A subset of ten rare earth element (REE) analyses were obtained by isotope dilution at SUNY, Stony Brook, on a 30.48 cm (12) radius, 90-sector mass spectrometer of NBS design (Bender et al., 1984) with precisions of 1.5% for Ce, Nd, Sm, Dy, Er and Yb and 2.5% for Gd and Eu. A further subset of 27 samples were analysed for the rare earth elements (REE), Ta, Hf, Th and U by Instrumental Neutron Activation Analysis (INAA) at Durham University on 0.2 g of powder irradiated for three days then counted, after 4 days for the short-lived isotopes and after 30 days for the long lived isotopes (Leat et al., 1987). Estimated precisions for these data at 1 ppm concentration are: Nd, Eu, Tb, Yb, Lu, Th, Ta and U 5%; La, Ce, Sm and Hf 10%. These data are presented in Table 3.

A total of 45 Sr isotope ratios were carried out (some duplicated), 30 at Oxford University and 32 at Leeds University; the former on a single-collector VG MM30 mass spectrometer, the latter on a VG MM54 mass spectrometer. Seventeen Nd isotope determinations were carried out at Leeds University on a VG MM33 mass spectrometer. Sr isotope ratios have all been normalized to $^{86}Sr/^{88}Sr = 0.1194$ and to the Eimer and Amend standard $SrCO_3$ value of $^{87}Sr/^{86}Sr = 0.70800$; analyses of the NBS 987 Sr standard during the period of analysis at Leeds gave a mean value of 0.71026 ± 2.1. Nd isotope ratios have all been normalized to $^{146}Nd/^{144}Nd = 0.7219$ for BCR 1 and to the La Jolla standard value of $^{143}Nd/^{144}Nd = 0.511046$. 2 σ errors are reported in both cases. These data are given in Table 4.

Eleven K – Ar age determinations were carried out on some key samples at the Department of Geophysics, Newcastle University on whole rock, crushed to between 1 mm and 355 μm, using the method described in Wilkinson et al. (1986). These data are given in Table 1.

The accuracy and precision of the geochemical data are comparable with the values given in the references cited. In the following sections we present new geochemical data and consider the major element, trace element, rare earth element and radiogenic isotope geochemistry of the various volcanic centres in order to constrain the processes involved in their genesis.

Classification of the volcanic suites using major element geochemistry

The collision volcanics cover a broad compositional spectrum from basalts to phonolites and rhyolites. The normative data for the basalts show silica saturation ranging from 5% nepheline normative to 2% quartz normative; in general, the samples with lower K contents are silica-oversaturated or silica-

TABLE 3

INAA and ID data for selected lavas from Eastern Anatolia

Volcano:	KARA	KARA	KARA	MUS	MUS	MUS	MUS	MUS	MUS	NEM	NEM	NEM	NEM
Sample:	1911	1913	1912	2113	2112	2115	2114	2111	2141	2411	2362	2313	2022
SiO_2(%)	46.7	48.8	50.2	47.5	50.1	51.2	52.0	53.7	66.2	48.5	47.7	64.2	64.3
La	17.25	17.59	18.94	23.48	28.60	54.52	41.91	35.41	41.88		14.36		43.26
Ce	47.72	48.96	48.68	62.18	77.74	139.86	116.47	90.74	113.06	102.00	44.37	86.60	100.91
Nd	23.25	21.82	26.95	32.38	44.10	62.75	47.34	45.75	57.10	55.20	23.62	40.10	47.25
Sm	5.21	5.13	4.89	7.07	8.45	14.27	11.24	8.92	11.06	11.90	5.56	8.72	10.33
Eu	1.58	1.47	1.78	1.90	2.40	3.64	2.94	2.33	1.63	3.72	4.41	2.52	5.99
Gd.										11.00		7.99	
Tb	0.62	0.48	0.76	0.87	1.13	1.70	1.48	1.07	1.16		0.92		1.09
Dy										10.10		8.88	
Ho	0.80	0.76	0.84		1.57						1.28		
Er										5.53		5.97	
Yb	1.41	1.23	1.69	3.07	4.00	5.16	5.54	4.41	4.47	4.74	3.04	5.55	5.44
Lu	0.24	0.23	0.24	0.45	0.61	0.83	0.73	0.61	0.80		0.45		0.71
U	0.23	0.33	0.38	1.10	0.73	1.74	0.91	1.71	7.68		0.23		1.84
Th	2.10	2.23	2.08	3.65	3.95	9.61	8.40	8.81	17.28		1.66		8.97
Ta	1.60	1.40	1.26	1.14	1.51	2.28	2.06	1.67	3.03		0.70		1.70
Hf	4.16	4.54	4.43	6.77	8.37	10.38	11.44	8.81	10.67		4.47		12.22

Volcano	NEM	BIN	BIN	BIN	BIN	SUP	SUP	SUP	TEN	TEN	ARA	ARA	ARA
Sample	2321	2213	2212	2211	2211	2521	2541	2541	3121	3111	3132	3031	3051
SiO_2(%)	74.2	55.4	58.2	71.1	71.1	62.8	73.1	73.1	48.9	58.4	51.1	56.6	57.1
La		28.52			36.53			39.90	50.64	58.62	18.90	26.85	23.51
Ce	150.00	67.18	65.10	66.60	76.27	65.10	86.30	82.03	126.30	128.41	52.72	67.79	54.38
Nd	61.60	23.98	26.70	21.00	25.22	31.00	33.10	30.74	58.50	50.92	26.64	29.11	22.73
Sm	13.80	4.61	5.04	3.47	3.72	6.77	5.57	6.40	10.34	8.53	5.17	5.50	4.32
Eu	0.32	1.25	1.43	0.75	0.78	1.98	1.33	0.75	2.88	2.41	1.63	1.62	1.39
Gd.	13.80		4.28	2.71		7.15	6.05						
Tb		0.59			0.45			0.84	1.35	1.34	0.69	0.53	0.53
Dy	16.60		4.53	3.14		7.69	6.67						
Ho											0.83		
Er	11.60		2.55	1.99		4.63	4.03						
Yb	11.20	2.43	2.32	2.07	2.27	4.40	3.97	3.78	4.75	5.28	2.46	2.74	2.12
Lu		0.35			0.34			0.63	0.76	0.93	0.41	0.46	0.36
U		2.47			6.42			6.40	0.96	3.73	0.30	1.99	0.95
Th		8.86			23.33			18.37	3.79	12.20	2.07	5.78	4.76
Ta		1.07			1.66			2.16	1.47	1.63	0.43	0.67	0.75
Hf		4.77			7.25			4.19	7.56	9.79	4.23	5.40	4.05

Volcano	ARA	ARA	ARA	KARS	KARS	KARS	KARS	KARS	KARS	KARS	KARS	KARS
Sample	3041	3131	3062	3011	2821	3021	2931	2921	2961	2911	2971	2811
SiO_2(%)	58.2	62.6	76.5	46.0	50.6	54.5	55.5	59.0	60.5	62.7	65.6	75.5
La	29.64		18.01		11.20	22.31	27.10	29.20	24.08		25.21	
Ce	64.07	47.30	40.15	46.40	29.57	54.70	62.55	65.57	55.08	47.1	56.27	45.3
Nd	25.75	20.60	16.66	27.50	15.92	23.47	24.78	23.20	19.99	18.9	20.47	15.8
Sm	4.41	3.96	3.23	6.17	4.23	4.38	4.59	4.38	3.79	3.79	3.11	3.16
Eu	1.36	1.22	0.46	2.05	1.34	1.32	1.37	1.20	1.16	1.06	0.98	0.35
Gd		3.48		5.60						3.3		2.79
Tb	0.51		0.50		0.68	0.74	0.63	0.69	0.43		0.53	
Dy		3.58		5.99						3.58		3.42
Ho					0.97							
Er		1.96		3.50						2.14		2.27
Yb	1.88	1.95	2.43	3.29	3.03	2.33	2.37	2.26	1.83	2.09	1.45	2.49
Lu	0.34		0.43		0.40	0.37	0.32	0.34	0.29		0.26	
U	2.20		2.63		0.34	0.79	0.81	2.05	1.27		2.04	
Th	6.29		7.16		2.58	5.88	5.08	7.77	5.18		7.06	
Ta	0.68		0.95		0.36	0.67	0.55	0.76	0.55		0.58	
Hf	4.05		2.99		3.20	3.60	4.46	4.90	4.69		3.65	

For analytical details, see text; for major elements and XRF/AA trace elements, see Table 2. *ARA* = Ararat; *TEN* = Tendürek; *BIN* = Bingöl; *SUP* = Süphan; *NEM* = Nemrut; *KARA* = Karacalidag.

saturated, while the samples with the highest K contents are silica-undersaturated. The volcanics have been classified here on the basis of their alkali and silica contents using the total alkali versus SiO_2 diagram of Le Bas et al. (1986) and the K_2O versus SiO_2 diagram of Peccerillo and Taylor (1976).

The total alkali versus SiO_2 diagram is shown in three parts in Figure 2 (a – c). The volcanic rocks from Nemrut, Mus and Tendürek plotted in Figure 2a contain high concentrations of alkalis at intermediate and high silica values and follow an alkaline trend. However, whereas Nemrut and Mus evolve to rhyolites and therefore lie on the silica-saturated side of the thermal divide, Tendürek contains strongly silica-undersaturated samples (a basanite and tephrite) and trachyandesites that plot on the silica-undersaturated side of the thermal divide. The foreland lavas of Karacalidag, also shown on this diagram, all classify as basalts. The Süphan and Bingöl samples plotted in Figure 2b form a well-defined trend from the trachybasalt to the rhyolite field, spanning the andesite-trachyandesite boundary at intermediate compositions and can be considered to be transitional between sub-alkaline (calc-alkaline) and mildly alkaline in character. The Kars and Ararat lavas plotted in Figure 2c fall predominantly

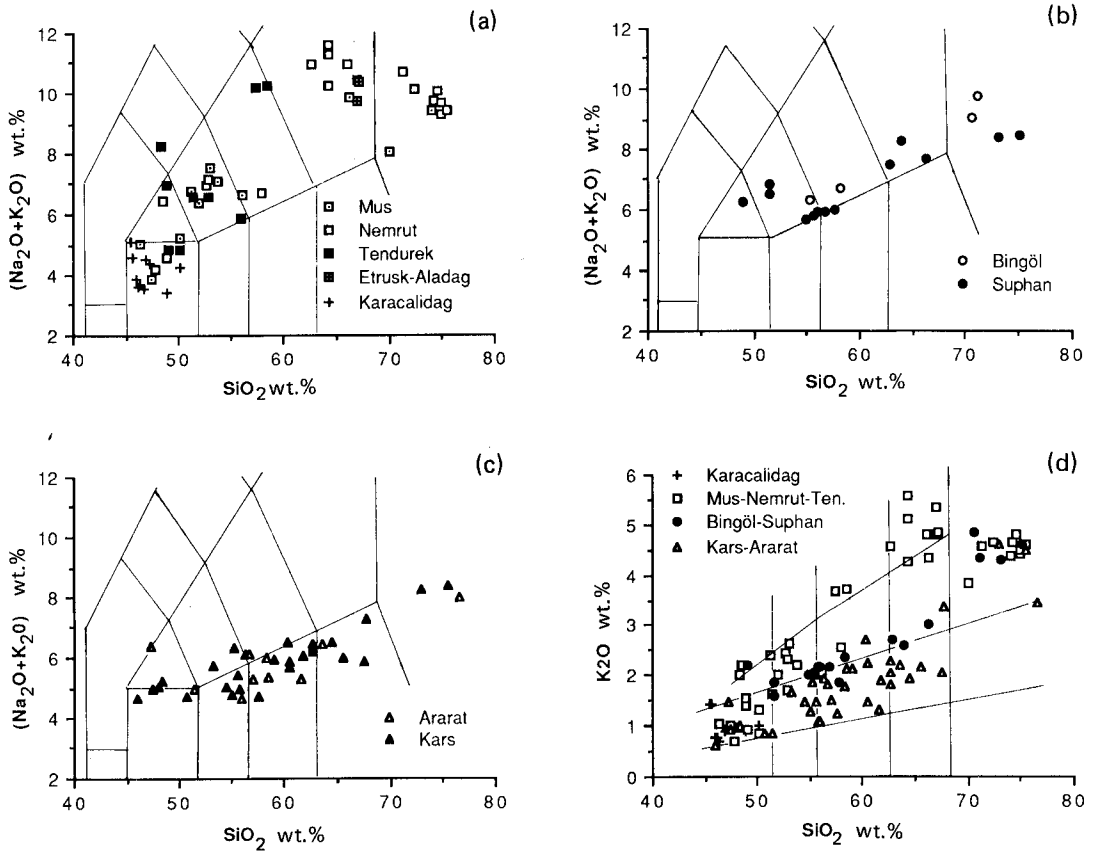

Fig. 2. Total alkali versus SiO_2 and K_2O versus SiO_2; classification boundaries after Le Bas et al. (1986) and Peccerillo and Taylor (1976), respectively; (a) highlights the alkaline character of Tendürek, Nemrut and Mus; (b) shows the mildly alkaline character of Süphan and Bingöl; (c) shows the sub-alkaline character of Kars and Ararat; and (d) shows the increase in potassium from the Kars – Ararat group, through the Süphan – Bingöl group to the Mus – Nemrut – Tendürek group.

TABLE 4

Sr and Nd isotope data for selected lavas from Eastern Anatolia

Volcano	Sample	Age (Ma)	SiO_2 (%)	Rb/Sr	$^{87}Sr/^{86}Sr$*	$^{87}Sr/^{86}Sr$**	$^{87}Sr/^{86}Sr)o$*	$^{87}Sr/^{86}Sr)o$**	Sm/Nd	$^{143}Nd/^{144}Nd$	ϵNd
KARA	1911	1.0	48.8	0.02	0.70398 ± 1	0.70388 ± 4	0.70398	0.70388	0.22	0.512948 ± 18	+6.05
KARA	1913	0.8	50.2	0.02	0.70451 ± 1		0.70451				
KARA	1912	0.9	58.0	0.36	0.70431 ± 1		0.70429		0.22	0.512887 ± 22	+4.86
BILC	2031	0.1	46.4	0.02	0.70402 ± 1	0.70390 ± 4	0.70402	0.70390			
MUS	2112	6.0	50.1	0.07	0.70432 ± 1		0.70429				
MUS	2114	5.0	52.0	0.13	0.70434 ± 1		0.70430				
MUS	2121	5.0	53.0	0.22		0.70463 ± 3		0.70457			
MUS	2111	5.0	53.7	0.15	0.70445 ± 1	0.70443 ± 4	0.70441	0.70439	0.19	0.512793 ± 19	+3.02
MUS	2141	5.0	66.2	0.51	0.70536 ± 1	0.70544 ± 3	0.70521	0.70529			
NEM	2362	0.1	47.7	0.02	0.70357 ± 1		0.70357				
NEM	2411	0.1	48.5	0.12	0.70559 ± 1	0.70525 ± 4	0.70559	0.70525		0.512850 ± 140	+4.14
NEM	2022	0.2	64.3	4.89	0.70630 ± 1	0.70608 ± 5	0.70624	0.70602			
NEM	2313	0.0	64.2	3.00	0.70620 ± 3	0.70617 ± 4	0.70620	0.70617	0.22	0.512772 ± 16	+1.64
NEM	2421	0.1	66.0	1.04		0.70505 ± 3		0.70504			
BING	2212	3.0	58.2	0.17		0.70473 ± 5		0.70470	0.19	0.512745 ± 25	+2.09
BING	2214	3.0	70.6	0.88		0.70506 ± 4		0.70491			
BING	2211	2.6	71.1	0.92	0.70518 ± 1	0.70512 ± 5	0.70504	0.70498		0.512795 ± 18	+3.06
SUP	2521	0.4	62.8	0.39		0.70505 ± 8		0.70504	0.29	0.512842 ± 18	+3.98
SUP	2531	0.2	63.9		0.70466 ± 1		0.70466				
SUP	2541	0.3	73.1	1.17	0.70537 ± 1	0.70535 ± 5	0.70535	0.70533	0.17	0.512968 ± 19	+6.44
ETR	2512	2.0	66.9	0.88	0.70537 ± 1	0.70531 ± 3	0.70527	0.70521		0.512808 ± 20	+3.32
ALA	3211	3.0	66.9	1.01		0.70630 ± 5		0.70612			
ALA	3221	3.0	67.2	0.83		0.70637 ± 6		0.70622			
TEN	3121	0.1	48.9	0.03	0.70567 ± 1	0.70563 ± 6	0.70567	0.70563			
TEN	3111	0.0	58.4	0.09	0.70536 ± 1	0.70534 ± 4	0.70536	0.70534	0.17	0.512816 ± 9	+3.47

TABLE 4 (continued)

Sr and Nd isotope data for selected lavas from Eastern Anatolia

Volcano	Sample	Age (Ma)	SiO_2 (%)	Rb/Sr	$^{87}Sr/^{86}Sr$*	$^{87}Sr/^{86}Sr$**	$^{87}Sr/^{86}Sr)o$*	$^{87}Sr/^{86}Sr)o$**	Sm/Nd	$^{143}Nd/^{144}Nd$	ϵNd
ARA	3132	1.5	51.4	0.02	0.70389 ± 1		0.70389				
ARA	3071	1.5	56.0	0.06		0.70443 ± 5		0.70442			
ARA	3031	0.5	62.6	0.11	0.70417 ± 1		0.70417				
ARA	3051	0.5	57.1	0.08	0.70465 ± 2	0.70453 ± 2	0.70465	0.70453	0.19	0.512909 ± 18	+5.29
ARA	3041	0.5	58.2	0.09		0.70416 ± 4		0.70416			
ARA	3131	0.1	62.6	0.15		0.70441 ± 5		0.70441			
ARA	3062	1.0	76.5	1.21	0.70397 ± 1	0.70376 ± 7	0.70389	0.70369	0.19	0.512976 ± 19	+6.59
KARS	3011	4.0	46.0	0.01	0.70380 ± 1	0.70374 ± 3	0.70379	0.70374			
KARS	2821	4.0	50.6	0.03	0.70362 ± 1		0.70362				
KARS	3021	4.0	54.5	0.07	0.70424 ± 1		0.70422				
KARS	2931	4.0	55.5	0.06	0.70415 ± 1	0.70411 ± 2	0.70414	0.70410	0.19	0.512974 ± 19	+6.55
KARS	2921	4.0	59.0	0.15	0.70429 ±		0.70426				
KARS	2941	4.0	60.2	0.15	0.70417 ± 1		0.70413				
KARS	2961	4.0	60.5	0.06	0.70408 ± 1	0.70395 ± 3	0.70407	0.70394	0.19	0.512875 ± 14	+4.62
KARS	PL2/15	4.0	61.7	0.07	0.70417 ± 1		0.70415			0.512939 ± 19	+5.87
KARS	2911	4.0	62.7	0.18		0.70415 ± 4		0.70411			
KARS	PL2/21	4.0	64.4	0.10	0.70418 ± 1		0.70416				
KARS	2971	4.0	65.6	0.13		0.70418 ± 3		0.70415			
KARS	PL2/14	4.0	72.9	8.09	0.70553 ± 1		0.70364			0.512948 ± 18	+6.05
KARS	2811	4.0	75.5	6.00		0.70553 ± 5		0.70413			

Abbreviations as for Table 2. See text for analytical details.
* leeds.
** Oxford.

into the sub-alkaline basalt, andesite, dacite and rhyolite (BADR) fields, a few samples just falling within the trachyandesite and trachyte fields.

The key features of the K_2O versus SiO_2 diagram are summarized in Figure 2d. Samples from Kars and Ararat predominantly classify as calc-alkaline on this diagram; Bingöl and Süphan are mainly high-K calc-alkaline; and Nemrut, Mus and Tendürek plot within the high-K calc-alkaline and shoshonite fields. The Karacalidag volcanics form a closely constrained group of basalts on the boundary between the calc-alkaline and high-K calc-alkaline fields.

Harker diagrams of major elements plotted against silica (not shown here) also demonstrate some significant differences between the Nemrut, Mus, Tendürek and Karacalidag samples on one hand and the Kars and Ararat samples on the other, with Bingöl and Süphan showing intermediate characteristics. Although there is some overlap at basic compositions, the former group is generally characterized by higher values of CaO and MgO at a given silica value and lower values of FeO, MnO and Na_2O. These differences are illustrated in Figure 3. Figure 3a highlights the high molar ratio of Ca to total alkalis in the Ararat and Kars samples at intermediate compositions (a ratio of 1 at about 60% SiO_2), confirming their calc-alkaline character. In contrast, intermediate lavas from Nemrut, Mus and Tendürek and from Bingöl and Süphan have lower ratios (a ratio of 1 at about 56% SiO_2) and hence a more alkaline character. It is beyond the scope of this paper to discuss these variations in detail although the fact that only the intermediate rocks discriminate in this way indicates that the differences are a function of fractionation: a greater proportion of clinopyroxene relative to hornblende as fractionating phases and greater crustal assimilation in the alkali suites could both contribute. Figure 3b shows the lower molar Mg/(Mg + Fe) ratios of the Ararat and Kars samples for a given silica content: the majority of data from these areas have values between 1.5 and 2.5 at 60% SiO_2 compared with a range of 3 – 6 for Süphan and Bingöl and 4 – 12 for Nemrut, Mus and Tendürek, up to SiO_2 values of around 65%. None of the volcanic suites follow Miyashiro's (1974) tholeiitic trend. The lower ratios in the intermediate Kars and Ararat samples may reflect the greater importance of amphibole, and lower importance of olivine and magnetite, in the crystallization assemblage; crustal assimilation may also have some effect. At higher levels of SiO_2, where iron is mainly in the trivalent state, the ratio decreases rapidly in all samples.

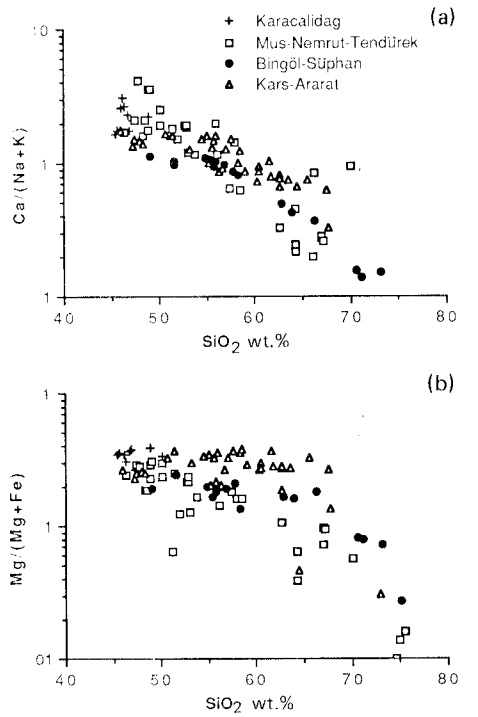

Fig. 3. Plots of calc-alkali ratio and Mg/(Mg + Fe) molar ratio against SiO_2. (a) shows the change from calc-alkaline character in the Kars – Ararat group, through the transitional character of the Süphan – Bingöl group to the alkaline character of the Mus – Nemrut – Tendürek group. (b) shows the absence of iron enrichment in all three groups, as well as the high Mg/(Mg + Fe) ratio in the calc-alkaline lava suites from Kars and Ararat.

Major and trace element evidence for fractional crystallization histories

Trace element fractionation trends

A subset of trace element analyses are plotted on log – normal graphs against SiO_2 to demonstrate some of the compositional differences between the different volcanic centres (Fig. 4). Most notably, Kars and Ararat volcanics are in general depleted in Zr, Y, Nb, Rb and Th and enriched in Sr, and Ni with respect to the Nemrut, Mus and Tendürek volcanics for samples of equivalent silica content; Süphan and Bingöl show features of both groups, having the abundances of the Mus – Nemrut – Tendürek group but generally following the fractionation trends of the Kars – Ararat group.

The behaviour of Y may be of particular significance. Y values for the basic rocks from all volcanoes overlap but there is a divergence of trends at intermediate compositions. For Kars and Ararat, Y stays broadly constant at basic – intermediate compositions; at higher SiO_2 values it either remains constant or is depleted. Lambert et al. (1974) used this trend to suggest amphibole ± garnet fractionation at depth beneath Ararat. They argued that Y is partitioned moderately strongly into hornblende – K_d = 1.0 at basic, 2.5 at intermediate and 6.0 at acid compositions (Pearce and Norry, 1979) – but not into other common crystallizing phases, and that there is no evidence in the behaviour of P or Zr for crystallization of the necessary proportion of minor phases such as apatite and zircon that might create the same effect. None of the samples analysed for this paper shows evidence for the fractionation of garnet (which occurs in a unit known as the Lower Red Tuffs, analysed by Lambert et al. (1974) but not sampled in this study), but our additional Y analyses support their model of amphibole fractionation, even though hornblende phenocrysts are only present as rare "ghosts". Süphan and Bingöl also follow a constant Y trend similar to that of Kars and Ararat but Nemrut, Mus, Bingöl and Tendürek all show an increase in Y with fractionation, consistent with a crystallization assemblage that includes neither amphibole, nor garnet. Zr and Nb behave in a similar, though less pronounced, way, increasing only slightly with increasing SiO_2 in Kars, Ararat, Bingöl and Süphan, while showing a constant increase for Nemrut, Mus, and Tendürek. This is again consistent with amphibole crystallization in the former group as both these elements partition into hornblende at intermediate and acid compositions (Pearce and Norry, 1979). Sr values decrease slightly with fractionation to acid compositions in response to plagioclase crystallization, then fall rapidly probably in response to the incoming of alkali feldspar as a crystallizing phase. Sr decreases more rapidly in the Nemrut – Mus – Bingöl – Tendürek group, indicating the greater importance of plagioclase crystallization in the origin of these rocks. Ni decreases steadily with increasing SiO_2 content in Kars and Ararat samples, but falls rapidly at low SiO_2 values for other suites, indicating that olivine fractionation is more important in the latter or that magma mixing is more important in the former. Of the elements plotted, only Rb and Th show a constant positive variation with SiO_2 for all the volcanic centres.

The behaviour of trace elements during fractionation can be studied more quantitatively by comparing observed and theoretical fractionation trends on log – log variation diagrams. The diagram Y – Rb, plotted in Figure 5 using both our own data and data of Lambert et al. (1974), highlights the main aspect of variation. Rb is used as a fractionation index because of its positive correlation with silica throughout the fractionation sequence. Theoretical Rayleigh fractionation vectors have been plotted for crystallization of individual phases and relevant phase assemblages using distribution coefficients from Irving and Frey (1984) and Pearce and Norry (1979). It can be seen that

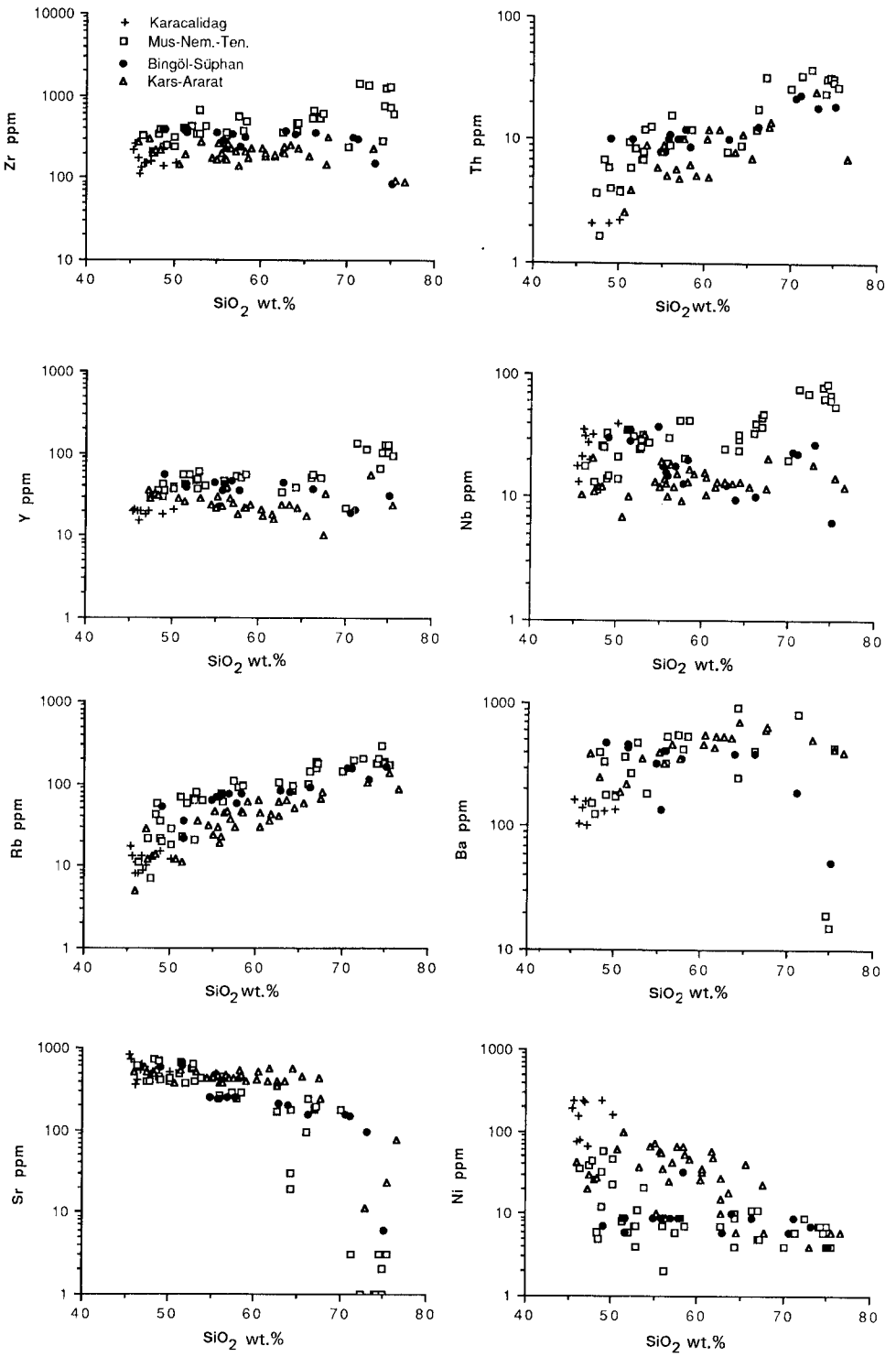

Fig. 4. Log–normal plots of Zr, Y, Nb, Th, Ba, Ni, Rb and Sr against SiO_2 showing the contrast in trace element behaviour between the calc-alkaline Kars–Ararat lavas and alkaline Mus, Nemrut and Tendürek lavas.

positive gradients on the diagram should generally result from POAM (plagioclase, olivine pyroxene, magnetite) fractionation, whereas negative to flat gradients require the crystallization of amphibole ± garnet ± biotite. Crustal assimilation (modelled in later diagrams) generally results in enrichment in Rb with depletion in Y and combined fractionation – assimilation will generally produce convex trends of increasing Rb and Y.

Three distinct trends can be recognized in Eastern Anatolia: the Nemrut – Mus – Tendürek trend of increasing Y and Rb which could be interpreted as dominated by POAM crystallization (resultant vectors 1 and 2); a Kars – Ararat trend (high-Y series) of near-constant Y best explained in terms of plagioclase- and amphibole-dominated fractionation (resultant vector 4); and a Kars – Ararat trend (low-Y series) best explained in terms of fractionation involving garnet (resultant vector 5). The Süphan – Bingöl trend shown in the inset mirrors the Kars – Ararat trends but is displaced to higher Y values.

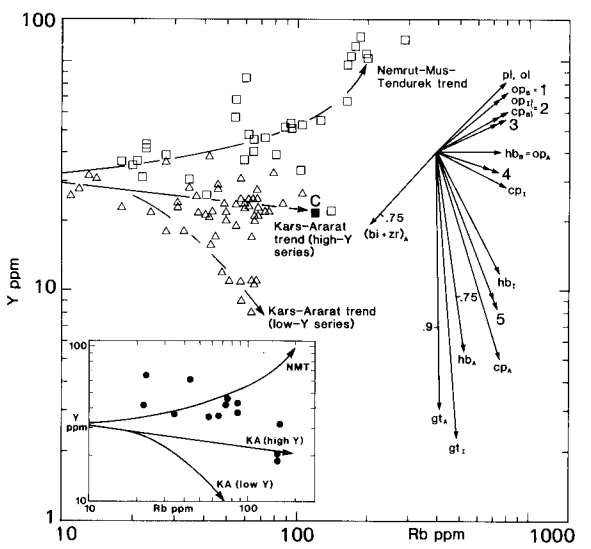

Fig. 5. Rb – Y diagram highlighting the contrast between the amphibole ± garnet dominated fractionation trends of Kars – Ararat (open triangles) and Bingöl – Süphan (closed circles in inset) and the POAM-dominated fractionation trends of Mus – Nemrut – Tendürek (open squares). Theoretical vectors are for 50% crystallization (unless otherwise stated) of single phases and phase combinations. Partition coefficients from Pearce and Norry (1979) and Irving and Frey (1984). *B* = basic; *I* = intermediate; *A* = acid. Phase combinations are: 1 = $pl_{.5}cpx_{.3}ol_{.2}$ (*B*); 2 = $pl_{.5}cpx_{.3}ol_{.2}$ (*A*); 3 = $pl_{.5}hbl_{.5}$ (*B*); 4 = $pl_{.5}hbl_{.5}$ (*I*); 5 = $pl_{.4}hbl_{.4}gt_{.2}$ (*I*).

The contrast in trace element behaviour, coupled with the phenocryst assemblages, can thus be seen to highlight the difference between hornblende-dominated fractionation in the calc-alkaline group and POAM fractionation in the alkaline group. The model of Lambert et al. (1974) for amphibole crystallization at depth beneath Ararat is thus consistent with our new data set and can also be extended to the Ararat – Kars area as a whole. The phase diagram considerations discussed by Lambert et al. (1974) also apply in the light of subsequent experiments such as those summarized by Green (1982) or Gill (1981). Thus, amphibole can be expected to be a liquidus phase in basaltic to basaltic – andesite magmas under near water-saturated conditions (> 10 wt.% H_2O at 15 kb) between depths of around 25 – 80 km (8 – 25 kb). At 25 – 40 km, within the thickened Eastern Anatolian crust, crystallization should initially be amphibole-dominated with subordinate aluminous pyroxenes and magnetite. Bringing the same magma to shallow depth would give two pyroxenes ± plagioclase as liquidus phases and cause any entrained amphibole crystals to be resorbed. This perhaps explains the general absence of hornblende in the dominant phenocryst assemblage of orthopyroxene, clinopyroxene, plagioclase, magnetite and ilmenite. Similarly, garnet can crystallize at depth (but not near surface) in intermediate to acid magmas.

Rare earth patterns

The chondrite-normalized REE data for representative lavas from the collision zone are shown in Figure 6 (a – g). The Karacalidag foreland basalts (Fig. 6a) have straight LREE-

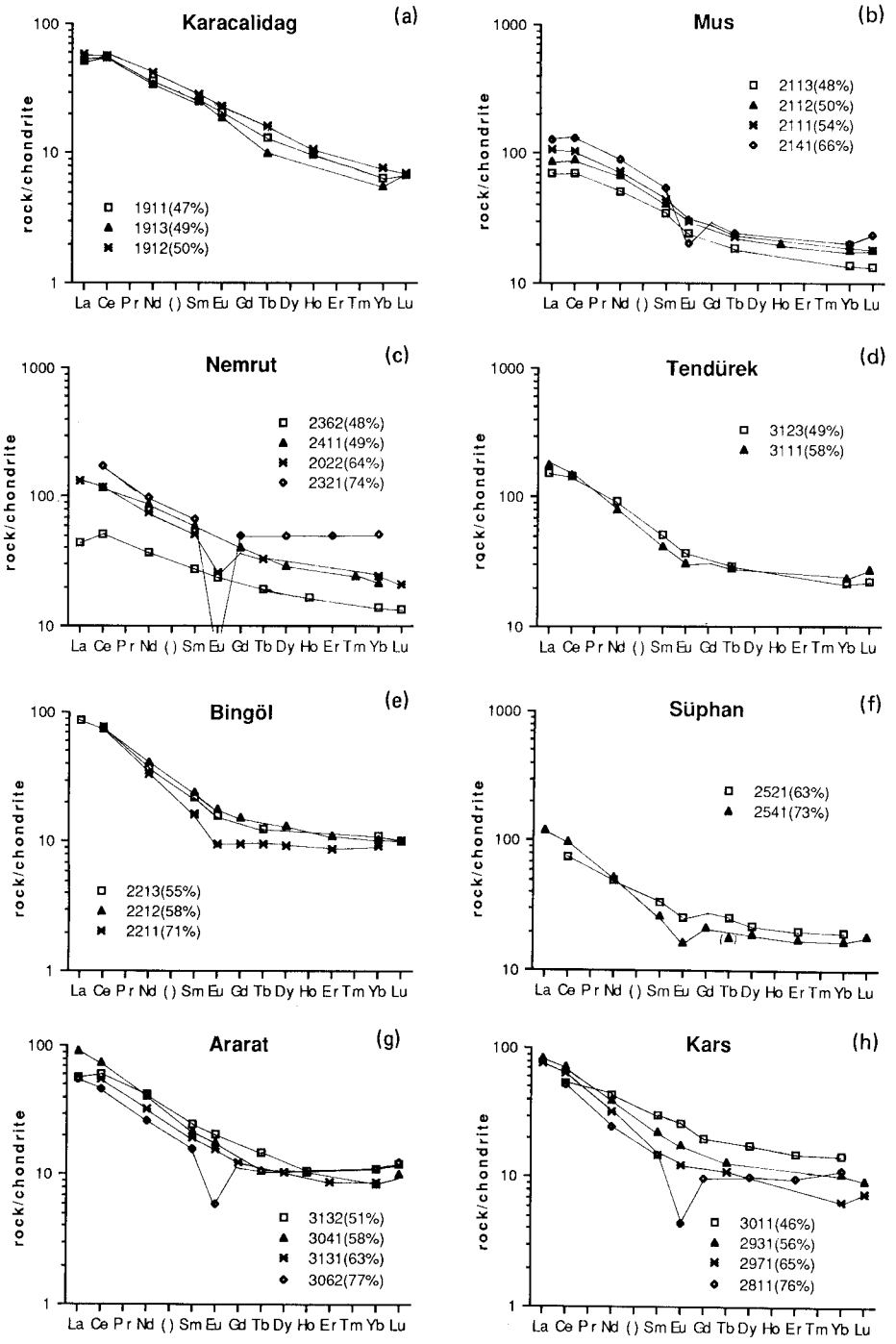

Fig. 6. Chondrite normalized REE plots for Karacalidag, Nemrut, Süphan, Tendürek, Ararat and Kars. The silica percentages of the samples are given in parentheses.

enriched patterns (we are not certain whether the slight depletion of La with respect to Ce is real or analytical) with LREE/MREE (as given by $La/Eu^*)_N$) and MREE/HREE (as given by $Eu^*/Yb)_N$) ratios both about 3 (Eu^* = extrapolated Eu). The mildly alkaline suites of Mus and Nemrut (Figs. 6b and c) have broadly similar patterns at basic compositions and then evolve to acid compositions showing little change in pattern shape (except at the very acid composition of Nemrut 2321) but an increasing negative Eu anomaly. The two samples plotted in Figure 6d from the alkaline Tendürek suite show higher LREE/MREE ratios (of 5 – 6) than the patterns so far described and little difference between the basic and intermediate patterns. These alkaline volcanoes have the highest total REE content (150 – 284 ppm at 50% SiO_2).

The calc-alkaline suites of the Kars Plateau and Ararat (Figures 6g – h) have similar LREE/MREE profiles to the alkali rocks at basic compositions but flatter MREE/HREE profiles (of 1.2 – 1.5). The trend to evolved compositions is the reverse of that seen in the alkali suites, however, with a general decrease in total REE content with increase in SiO_2 content and much less pronounced Eu anomalies for a given SiO_2 content. The greatest decrease is shown by the M – HREEs, which are partitioned most strongly into amphibole; the LREEs, La and Ce, exhibit variable behaviour. Süphan and Bingöl patterns (Figs. 6e and f) resemble the calc-alkaline, rather than alkaline, patterns in their total REE content and fractionation behaviour.

Rare earth patterns thus also highlight the contrast between the amphibole-free, and more hydrous, amphibole-bearing crystallization histories. The former, characterized by Mus and Nemrut, where the acid rocks have patterns that lie sub-parallel to the patterns of the basic rocks and have large negative europium anomalies, are typical of other volcanoes exhibiting POAM fractionation. The latter, exemplified by Kars, Ararat, Bingöl and Süphan, where there is no increase or a decrease of the MREE and HREE during fractionation, are consistent with amphibole-dominated crystallization assemblages.

Summary

The evidence presented above enables us to propose that there are two distinct types of crystallization history:

(1) The Kars and Ararat type is characterized by subalkaline basalt – andesite – dacite – rhyolite fractionation, high ratios of calcium to total alkalis and magnesium to iron, and trace element data that show either constant trends or trends of depletion in Y, Zr and Nb with fractionation. These features are consistent with crystallization of a hydrous (amphibole ± garnet bearing) assemblage at depth. Süphan and Bingöl, which are transitional between groups 1 and 2, also have an amphibole-dominated crystallization history.

(2) The Nemrut and Mus type is characterized by alkaline compositions that follow basalt – trachyandesite – peralkaline rhyolite fractionation trends. They have low ratios of CaO to alkalis and magnesium to iron and show increases in Zr, Y and Nb throughout their fractionation history. These features are consistent with an anhydrous (POAM) crystallization assemblage. Tendürek also belongs to this group but does not evolve to peralkaline rhyolite and has more silica-undersaturated compositions.

Incompatible trace element evidence for the nature of the mantle source regions

Multi-element patterns

More complete incompatible element trace element patterns, normalized to MORB after Pearce (1983), are shown in Figure 7 and have been used to contrast source compositions across the volcanic province. In these patterns, the order of incompatibility during lherzolite melting increases from Yb to Th and Sr to Th.

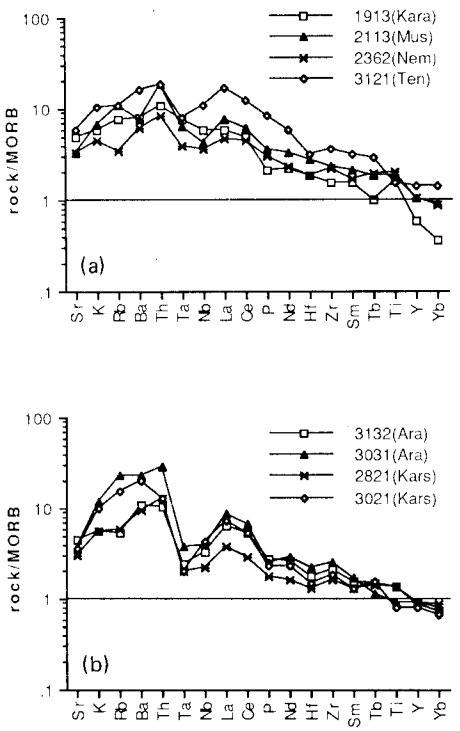

Fig. 7. MORB-normalized patterns (after Pearce 1982) for basic samples from Karacalidag, Tendürek, Mus, Nemrut, Ararat and Kars; only the Kars – Ararat samples show a consistent subduction signature.

Comparison of a number of basalt patterns has suggested that melting of "plume" asthenosphere, or lithosphere enriched by small-volume melts from the asthenosphere, produces "humped" patterns with Ba, Th, Ta and Nb the most enriched elements and the degree of enrichment directly relating to the degree of incompatibility. By contrast, basalts derived from mantle enriched by a subduction component exhibit selective enrichment mainly in the large ion lithophile (LIL) elements Sr, K, Rb, Ba, Th and the LREEs. These patterns best highlight source enrichment processes when pyroxene, plagioclase and oxides are the only residual phases during partial melting and are also the only crystallizing phases. Crustal assimilation can have the same, but less pronounced, effect as the subduction component, leading to LIL element enrichment. If garnet is a residual phase, Y and the M – HREE (Tb, Y, Yb) will be depleted. Amphibole crystallization will also significantly "hold back" K, Y and the M – HREE and slightly "hold back" Sm, Ta and Nb. To reduce the latter effect, only basalts have been plotted in Figure 7.

In Figure 7a, the Karacalidag pattern characteristic of the foreland volcanism, shows a "humped" trace element pattern enriched in both the LIL elements, Sr, K, Rb, Ba, Th and the LREEs and the incompatible high field strength (HFS) elements Ta, Nb, Hf, Zr, and Ti relative to the MORB normalizing abundance. This can be interpreted in terms of a mantle source with significant enrichment of a small-volume asthenospheric melt and an insignificant subduction or crustal assimilation component. The alkali basalts from Mus, Nemrut and, especially, Tendürek also show "humped" patterns but with a small, but variable, depletion of Ta and Nb relative to the adjacent LIL elements that characterizes a small subduction component in the mantle source or assimilation of crust by the basic magma prior to eruption. The Karacalidag pattern also shows a marked depletion of Y and the heavy REEs that may indicate that garnet was a residual phase during the partial melting event; the other volcanoes do not show this feature.

The Kars and Ararat basalts in Figure 7b show only slight enrichment in the HFS elements relative to the MORB normalizing abundance ($1-2 \times$ MORB), with selective enrichment of the LIL elements, Sr, K, Rb, Ba, Th and the LREEs giving negative anomalies in Ta and Nb that are much larger and more consistent than those in the alkali volcanoes. The slight enrichment in the incompatible HFS elements such as Nb and Ta relative to MORB may indicate a slightly enriched mantle source (it may also be produced in part by partial melting if the degree of melting is small and clinopyroxene is a major residual phase); whereas the pattern of selective LIL element enrichment can be attributed either to a sub-

duction component or to crustal contamination or both. Bingöl and Süphan exhibit similar features at intermediate compositions, but no basic rocks from these volcanoes have been analysed for all elements.

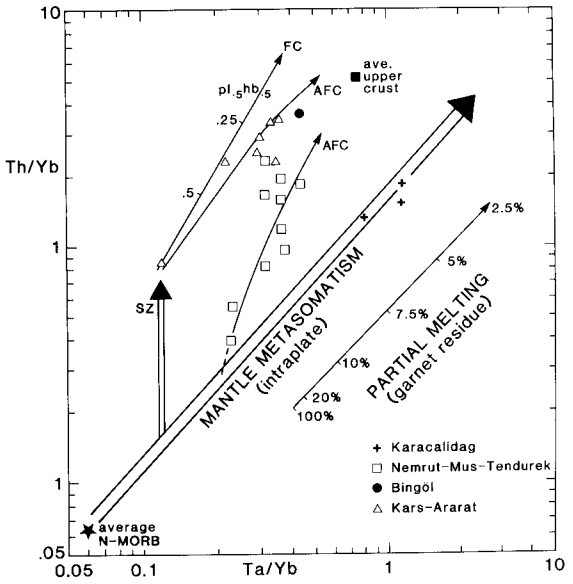

Fig. 8. Th/Yb – Ta/Yb diagram (after Pearce, 1983) for basic and intermediate (< 60% SiO_2) lavas from Eastern Anatolia. The foreland lavas from Karacalidag plot on an intraplate mantle metasomatism trend, whereas the Kars – Ararat lavas exhibit a consistent displacement from the trend indicating subduction-related metasomatism. The alkaline volcanic series of Nemrut, Mus and Tendürek exhibit a progressive shift from this trend with increasing silica, indicating a parent composition on or near this trend that has evolved via combined assimilation – fractional crystallization (AFC). Possible subduction zone (SZ), fractional crystallization (FC) and AFC vectors are indicated. The FC vector for the Kars – Ararat lavas is modelled for a hornblende – plagioclase assemblage; FC vectors for the alkaline series involving plagioclase, pyroxene and magnetite are negligible on the scale of the diagram and have not been drawn. AFC vectors are drawn for values of $r = 3$ (see text) and the upper crustal composition of Taylor and Mc-Lennan (1985). The partial melting trend has been modelled for equilibrium melting of a garnet lherzolite ($ol_{.55}opx_{.2}$, $cpx_{.15}gt_{.10}$) assemblage melting at 1250°C (see text for details) and is annotated according to degree of melting: it shows that the high ratios of the Karacalidag lavas could be explained by a more enriched source than the uncontaminated alkaline volcanoes and/or by a very low degree of melting.

Trace element ratio plots

The main variations shown by the trace element patterns can be summarized by a plot of Th/Yb against Ta/Yb (Fig. 8). This choice of ratios is designed to be almost independent of fractional crystallization or partial melting, provided pyroxenes and feldspars are the dominant crystallizing or residual phases; and to highlight source variation and crustal assimilation (Pearce, 1983). Basalts derived from the convecting upper mantle (MORB source), "plume" asthenosphere or lithosphere enriched by low-degree melts from the convecting upper mantle all lie within or close to a diagonal trend marking the similar behaviour of Th and Ta. Mantle enriched by a subduction component (carrying Th but not Ta or Yb) will be shifted off the appropriate point on this array to higher Th/Yb ratios. Bulk or partial assimilation of most crust also leads to a shift to higher Th/Yb ratios, although assimilation of granulite facies crust, which has low Th contents, can cause a shift in the opposite direction. Garnet residues from partial melting should lower both ratios by similar amounts, and amphibole residues will lower Ta/Yb slighly more than Th/Yb: crystallization of these phases will have the reverse effect.

The diagram shows that the Karacalidag basalts plot on the "mantle trend", confirming the interpretation from the trace element patterns that the enriched mantle source had no subduction component and that the resulting magma underwent little assimilation. The alkaline volcanoes Mus, Nemrut and Tendürek follow a trend from the mantle array to higher Th/Yb ratios. The degree of displacement correlates with the silica content, which is consistent with a model of variable crustal assimilation of an enriched mantle source. The Karacalidag basalts are displaced along the "mantle trend" to higher Th/Yb and Ta/Yb ratios. This displacement could be explained by derivation from a more enriched source than that of the alkaline volcanoes, or to the pres-

ence of a garnet-bearing residue in the genesis of the Karacalidag basalts. The garnet lherzolite melting trend (for garnet out at 20% melting at 1250°C – see Fig. 9) shows that a large difference in the proportion of residual garnet (and hence degree of partial melting) is needed to explain this observation; a combination of the two explanations may therefore be involved. The Kars and Ararat lavas form a trend subparallel to the "mantle array", but consistently shifted to higher Th/Yb ratios, suggesting derivation from an enriched mantle source to which a subduction component has been added. The basic rock has the lowest ratio; the intermediate rocks which form the main group of data could be derived from the basic lava by amphibole fractionation (FC vector, Fig. 8) with or without crustal assimilation (sub-parallel to the AFC trend, Fig. 8). There are insufficient data on basic and intermediate rocks from Bingöl and Süphan to assess their origin.

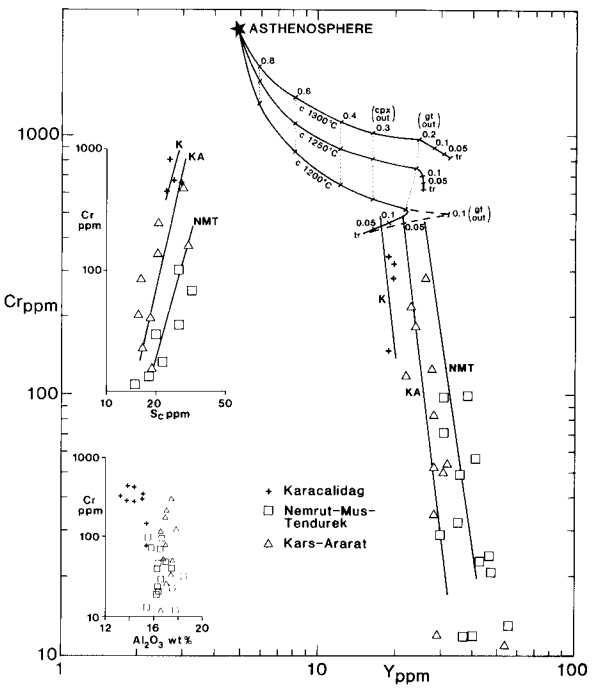

Fig. 9. Cr – Y diagram (with Cr – Sc and Cr – Al_2O_3 diagrams in insets) highlighting differences in degree of partial melting between the different volcanic series. The modelling of the partial melting trends is based on an $ol_{.55}opx_{.2}cpx_{.125}gt_{.125}$ assemblage with garnet disappearing after 20% melting (except at 10% where indicated), clinopyroxene after 30% melting and orthopyroxene after 60% melting. Mineral/melt partition coefficients used for Y are: 1200°C: ol = .005, opx = .06, cpx = .5, gt = 2; 1250°C: ol = .002, opx = .03, cpx = .3, gt = 1.5; 1300°C: ol = .001, opx = .01, cpx = .2, gt = 1.0. Distribution coefficients for Cr result in almost constant bulk distribution coefficients during melting, namely: 1200°C = 6; 1250°C = 4; 1300°C = 3. For details, see text.

Compatible – incompatible element covariations: evidence for degree of partial melting

The depletion in Y and the M – HREE shown by the Karacalidag lavas in Figure 7a can be examined further by a plot of the compatible element, Cr, against Y (Fig. 9). This diagram is not greatly affected by source heterogeneities (small melt fractions in equilibrium with garnet will be depleted in Cr and exhibit only a small enrichment in Y) but will highlight differences in degree of partial melting – which form a horizontal trend on this diagram almost perpendicular to the sub-vertical trend formed by crystallization of assemblages dominated by olivine, chrome spinel, pyroxene and/or hornblende (Pearce, 1982). In the simple model drawn in Figure 9, we have assumed that the mantle source has the same Cr, Y content as "normal" convecting asthenosphere, i.e. that mantle metasomatism has not affected the two elements significantly and the lithosphere has not experienced a previous melting event. The melting trends drawn are for garnet lherzolite, ignoring the effects of residual hydrous phases and carbonates which are expected from experiments to enter the melt very rapidly (e.g. Olafsson and Eggler, 1983). Because of the strong temperature-dependence of the partition coefficients, three melting trends have been plotted, for temperatures in the order of 1300°C, 1250°C and 1200°C (synthesized from published data and reviews, especially Irving, 1978; Ottonello et al., 1984; Hervig et al., 1986,

treating Y as equivalent to a M – HREE). In practice, a single melting trend would steepen with the degree of melting as the partition coefficients decrease and the trends assume equilibrium melting. In addition, the precise temperature-dependence of the partition coefficients is poorly known. However, the diagram does serve to constrain melting models for the Eastern Anatolian lavas because of the general trend of increasing Y in primary melts generated from increasing degrees of partial melting of garnet lherzolite at temperatures below those of convecting asthenosphere (i.e. below about 1300°C) and at degrees of melting where garnet is a residual phase.

Using this diagram, back-projection along a mafic crystallization trend would cause the Karacalidag lavas to intersect a melting trend at lower Y values than the Kars – Ararat lavas, which in turn would intersect the partial melting trend at lower values than the alkaline volcanic rocks of Nemrut, Mus and Ararat. The diagram therefore provides good evidence for a difference in degree of melting or nature of the melt residue across the volcanic province even though the precise details are difficult to determine. The theoretical trends show that the lower Y contents of the foreland Karacalidag lavas could be explained if garnet was a residual phase and the Karacalidag lavas had undergone a lower degree of partial melting than the lavas from the zone of crustal thickening. An alternative model for this diagram is that the Karacalidag lavas had undergone a much higher degree of partial melting and that neither garnet nor clinopyroxene were residual phases, although this would require temperatures in excess of those of "normal" convecting asthenosphere to generate sufficient melt by adiabatic decompression.

Further evidence is provided by the behaviour of Sc and Al, shown as insets in Figure 9. Sc is strongly partitioned into both garnet and clinopyroxene (K_d for clinopyroxene/melt and garnet/melt = 3 – 6) so its concentration increases in primary melts as the degree of melting increases until there is a harzburgite residue, at which point its concentration in the melt decreases. Its concentration in primitive MORB lies in the range of 35 – 40 ppm but is in the order of 25 ppm in the most basic of the volcanics from the EACZ, suggesting that overall degrees of melting and/or melting temperatures were less than those required to generate MORB. Furthermore, the extrapolated value is lowest in the foreland Karacalidag volcanics, consistent again with a lower degree of partial melting for the generation of these lavas. Similarly, the low contents of Al_2O_3 in the Karacalidag lavas compared with the other volcanic suites supports the model of their generation by low degrees of melting with residual garnet.

Isotope evidence for crustal assimilation

Isotope – trace element diagrams

The question of source enrichment versus crustal contamination, not fully resolved by the trace element variations, can be further studied from Sr isotope covariations with indices of fractionation using data from Table 4. The diagram of $^{87}Sr/^{86}Sr$ against SiO_2 (Fig. 10a) highlights a significant linear or curvilinear correlation between Sr isotope ratios and silica for all the alkaline volcanic suites (Mus, Nemrut and Tendürek) from the area of thickened crust, suggesting that the combined assimilation and fractional crystallization (AFC) was an important process in the origin of these volcanoes. A few samples plotting off this AFC trend include two highly alkaline basic Tendürek samples with high Sr isotope ratios and one Nemrut basalt with a slightly low ratio that may indicate a variability in primary melt compositions. The Nemrut sample 2362 plots at the lower end of the trend, and is used as the basic end-member in subsequent AFC modelling; the foreland Karacalidag volcanics also plot near the low-silica end of the trend. The transitional volcanoes (Bingöl and Süphan) also show a small increase in Sr isotope ratios with silica,

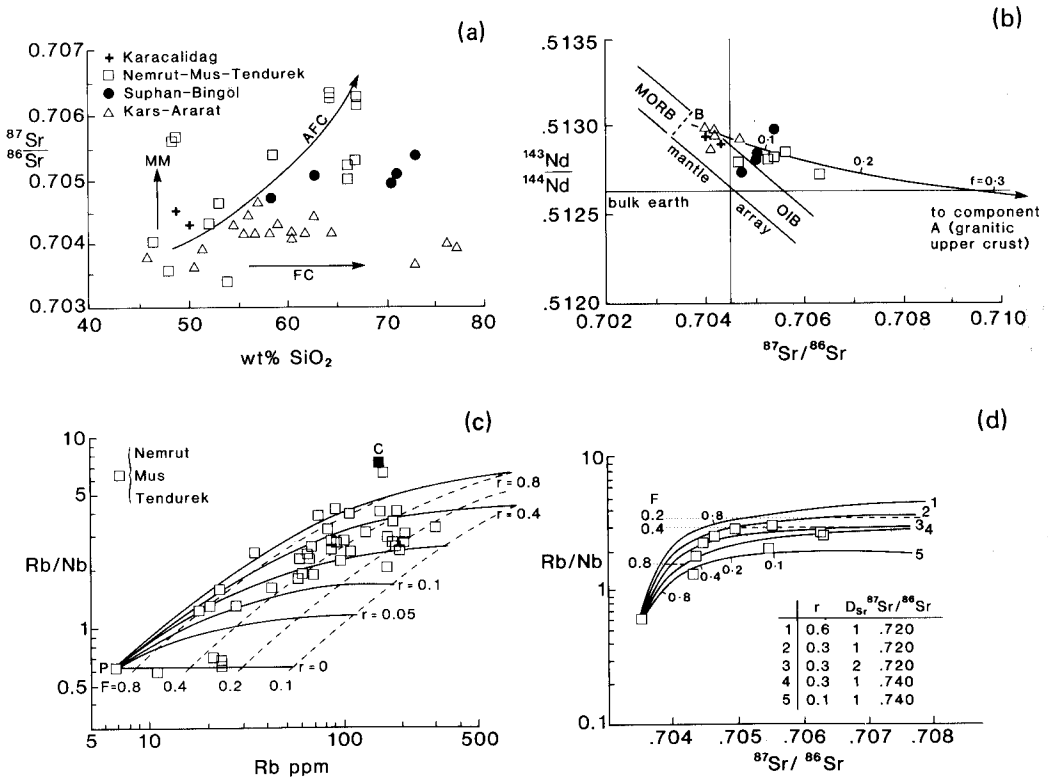

Fig. 10. Diagrams highlighting assimilation – fractional crystallization (AFC) processes in the alkaline volcanics of Mus, Nemrut and Tendürek. (a) Increase in Sr isotope ratio with silica for the alkaline suites along a generalized AFC trend, with the exception of two samples that plot on a mantle metasomatism (MM) trend. The Kars – Ararat lavas mostly plot along a fractional crystallization (FC) trend. (b) The Sr – Nd isotope covariation shows that alkaline lavas are displaced from the mantle array along a two-component mixing line. *B* = Columbia River Basalt; *A* = average NSW granite of Faure (1986) annotated according to the proportion (*f*) of component *A*; (c) and (d) More detailed modelling of the AFC process based on the equations of De Paolo (1981) and using the assimilation-sensitive ratio Rb/Nb. *r* = the ratio of the rates of mass assimilation to mass crystallization and *F* = the ratio of magma mass to original magma mass. *C* = Rb, Nb composition of the upper crust; $^{87}Sr/^{86}Sr$ in the table in (d) = Sr isotope ratio of the assimilated crust.

but the number of data points is insufficient to determine their significance. The Kars – Ararat calc-alkaline group follows a line of constant Sr isotope ratio from basaltic andesite to dacite composition. This may indicate a fractionation-dominated history, or that the magmas assimilated young crust of similar Sr isotope ratio. The three basic samples have lower Sr isotope ratios than the intermediate rocks (0.7038 compared with 0.742) showing that the basic and intermediate rocks cannot be related simply by fractional crystallization. The acid samples, however, have Sr isotope ratios which are more comparable to those of the basic lavas.

Nd – Sr isotope diagram

A Sr and Nd isotope covariation diagram has been plotted in Figure 10b using data from Table 4. The Nemrut, Süphan, Tendürek, Mus, and Bingöl lavas are almost all displaced from the mantle array, showing a considerable spread in their $^{87}Sr/^{86}Sr$ ratios with a relatively small range of $^{143}Nd/^{144}Nd$ ratios (0.51270 – 0.51285). The Kars and Ararat lavas form a se-

cond group which has lower $^{87}Sr/^{86}Sr$ (0.7036 – 0.7047) and higher $^{143}Nd/^{144}Nd$ (0.51288 – 0.51298). The two Karacalidag data points plot together on the edge of the mantle array with $^{87}Sr/^{86}Sr$ ratios between about 0.7040 and 0.7042 (in addition, one sample, not analysed for Nd isotopes, has a $^{87}Sr/^{86}Sr$ ratio of 0.7045) and $^{143}Nd/^{144}Nd$ ratios between about 0.51289 and 0.51295. Samples not following an AFC trend in Figures 10a and b plot closest to the mantle array, and make up a trend parallel to the mantle array, the alkaline Tendürek sample being most enriched. Precise interpretation of this trend, particularly the separation of a subduction and intraplate enrichment component in the Ararat – Kars group, is not possible at this stage.

Samples from Mus, Nemrut and Tendürek that followed an AFC trend in Figure 10a, form a trend towards upper crustal compositions. Not having sufficient information to define precise end-member compositions for this trend, a simple two-component mixing curve between a composition similar to the Karacalidag basalts – Component *B*: the Columbia River Basalt of Carlson et al. (1981) – and a possible bulk upper crustal composition – Component *A*: SE Australia Palaeozoic granite average of McCulloch and Chappell (1982) – has been drawn onto the diagram to indicate the extent of mixing that might have taken place (Faure, 1986). This curve gives bulk weight fractions (*f*) of component *A* up to about 0.15. One representative sample of the Bitlis metamorphic rocks (a phyllite sampled east of Tatvan) analysed at Oxford gave values of Rb = 130 ppm, Sr = 69 ppm and $^{87}Sr/^{86}Sr = 0.73586 \pm 5$; similar in composition to the upper crustal estimate used in Figure 10. No clear trend is shown by Bingöl and Süphan on this diagram; however, Gülen (1980, 1982) reported that his larger isotopic data base for Süphan does provide strong evidence for crustal assimilation.

More rigorous modelling of the AFC process for the Mus – Nemrut – Tendürek group of volcanoes has been attempted in Figures 10c and d. The Rb/Nb ratio has been chosen as an index of assimilation for these suites because POAM crystallization should not fractionate this ratio significantly whereas crustal assimilation should cause the ratio to increase. The Nemrut sample 2362 has been chosen as the basic end member of these models, partly because it plots at the end of the AFC trend in Figure 10a and partly because its Rb/Nb ratio of 0.6 is similar to the Rb/Nb ratio of MORB and many ocean islands and can therefore be considered unaffected by assimilation. Values of Rb = 150 and Nb = 20 (similar to the representative Bitlis pelite) have been used to represent the assimilated crust. Modelling has been carried out using the AFC equations of De Paolo (1981) assuming bulk distribution coefficients of 0.1 for Rb and Nb throughout the crystallization history (the model is not sensitive to changes in these values provided they are $<< 1$).

Figure 10c shows a diagram of Rb/Nb ratio against Rb for the volcanic rocks of Mus, Nemrut and Tendürek, upon which has been superimposed theoretical curves to illustrate how the basic end member would evolve by AFC for different values of r, the ratio of assimilation rate to crystallization rate; the value of F (the ratio of the final mass of magma to the initial mass of magma) has been marked onto each curve. The Figure highlights two features. First, a small number of samples plot along the theoretical trend for $r = 0$, indicating little or no crustal assimilation. The trend shown by these samples, of increasing Rb at a constant Rb/Nb ratio, can be explained by fractional crystallization alone, or by source heterogeneities, or both. Since the samples in question are all basic in composition, and two of the high-Rb samples are the Tendürek samples that have high Sr isotope ratios (Figure 10a), this trend must reflect source heterogeneities, at least in part. It can therefore be inferred that a small proportion of lavas from these volcanoes reached the surface without ex-

tensive assimilation and without the extensive mixing in crustal magma chambers that might have homogenised their isotopic and trace element variations. The remaining lavas, the dominant set, plot on AFC trends with values of r from 0.1 to 0.8, but mainly in the range 0.15 – 0.4. The precise values of r are not very meaningful, because of potential variations in end-member compositions. For example, taking the average upper crustal composition of Taylor and MacLennan (1985) (Rb = 112 ppm; Nb = 25 ppm) as the crustal end-member would cause the estimates of r to be revised slightly upwards. Taking into account the fact that the Nemrut end-member is itself fractionated, and that its primary magma should have a lower Rb content, would cause the values of r to be revised downwards; and taking one of the more enriched basic end members would cause the value of r to be revised upwards. There is no evidence that any granulitic (low-Rb) crust, if indeed it is present in Eastern Anatolia, was assimilated.

A comparable diagram has been constructed for the Rb/Nb ratio against the Sr isotope in Figure 10d. The curves drawn, again from the equation of De Paolo (1981), encompass the expected range of values of $r = 0.1 - 0.6$, $D_{Sr} = 1 - 2$, and $^{87}Sr/^{86}Sr = 0.720$ and 0.740. Although based on fewer data points than the previous diagram, this plot supports the model of extensive crust assimilation within the collision zone.

In terms of the process, there may be strong similarities between Eastern Anatolia and the Central Chilean Andes, for which Hildreth and Moorbath (1988) proposed a blending of subcrustal and deep crustal magmas in zones of melting, assimilation, storage and homogenisation (MASH) at the mantle – crust transition. There is no evidence in Anatolia for the blending of acid and basic *magmas*, but the data from the alkaline volcanoes (where the isotopic and trace element contrast between magma and crust is largest) do indicate that extensive combined assimilation and fractional crystallization of crust is taking place at depth beneath Eastern Anatolia, and that only a small volume of basic magmas has avoided these magma reservoirs and reached the surface in an uncontaminated state.

Models for Eastern Anatolian volcanism

Foreland volcanism

The Karacalidag lavas on the Arabian foreland provide the control on magma genesis without the effects of lithospheric thickening and can usefully be discussed first in terms of the $P - T$ relationships of mineral stabilities, mantle solidi and geothermal gradients. The constraints identified so far are that they are: (1) predominantly basic; (2) mildly alkaline; (3) characterized by anhydrous fractionation phases; (4) have trace element and isotope ratios which indicate a slightly enriched mantle source with little or no subduction component; (5) may have been generated by low degrees of melting leaving some residual garnet; (6) have experienced little or no crustal contamination.

We have assumed that the foreland structure prior to volcanic activity (Fig. 11) is represented by typical, non-cratonic, continental lithosphere with a 100 km, rigid, mechanical boundary layer (MBL) separated by a thermal boundary layer (TBL) of variable thickness (taken here as 75 km) from convecting asthenosphere. The MBL is assumed to have a linear (conductive) geotherm of mean gradient 9°C km^{-1} and the asthenosphere an adiabatic gradient of 0.6°C km^{-1} with a potential temperature, T_p (the temperature it would have if brought adiabatically to the surface without melting), of 1280°C. The dry asthenosphere solidus is taken from figure 5 of McKenzie and Bickle (1988). The solidi for the peridotite – H_2O – CO_2 system are taken from Wyllie (1987) and show the minimum temperatures of magma generation from metasomatized lithosphere in the range X_{H_2O} ($H_2O/(H_2O + CO_2)$ = 1 and X_{CO_2} ($CO_2/(H_2O + CO_2)$) = 1. The MBL is

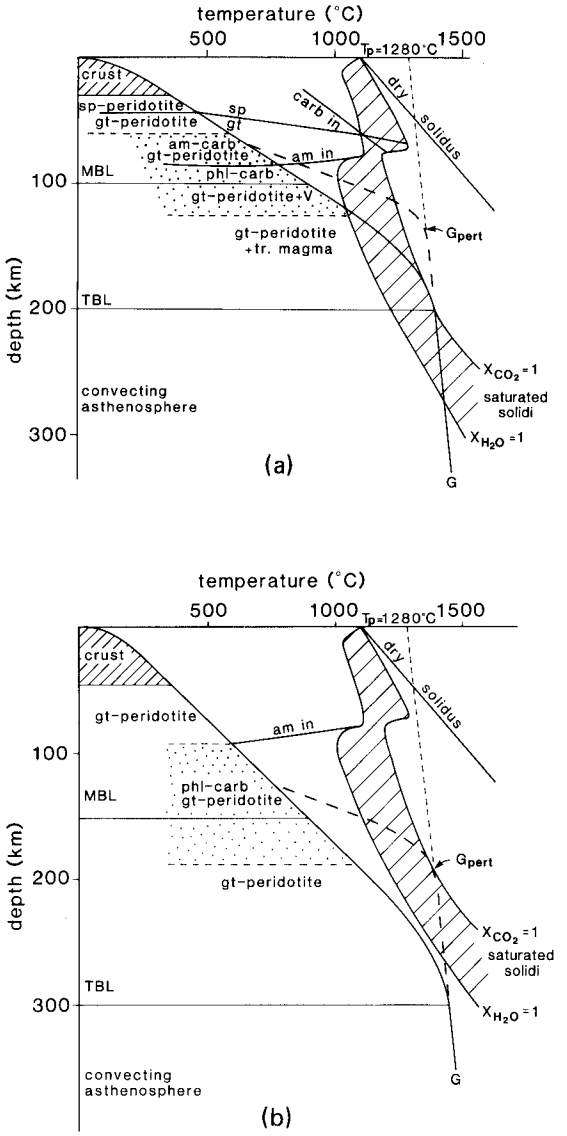

Fig. 11. $P-T$ diagrams showing conditions of melting across the Eastern Anatolian volcanic province. (a) The foreland (pre-thickening) lithosphere. (b) The thickened lithosphere for the EACZ. *MBL* = mechanical boundary layer; *TBL* = thermal boundary layer; G = continental geotherm; G_{pert} = perturbed geotherm; T_p = potential temperature; shaded region = field of initiation of melting for volatile-rich compositions ranging from pure water ($X_{H_2O} = 1$) to pure carbon dioxide ($X_{CO_2} = 1$). Mantle compositions on the geotherm: *sp* = spinel; *gt* = garnet; *am* = amphibole; *carb* = carbonate; *phl* = phlogopite; are given, assuming that metasomatized compositions lie between the dotted lines. For details, see text.

assumed to have been metasomatised at depths below the intersection of the geothermal gradient and the metasomatised lithosphere solidus by small melt fractions migrating from the asthenosphere to the lithosphere along the geothermal gradient (Bailey, 1987). Consideration of mineral stabilities then gives a mineralogically zoned, metasomatized MBL mantle lithosphere from hornblende (garnet or spinel) lherzolite at shallow depths through hornblende, dolomite (garnet, phlogopite) lherzolite to carbonate, garnet, phlogopite lherzolite at the base (Wyllie, 1987; Bailey, 1987). Potential end-member magma sources are: the main volume of "normal" convecting upper mantle asthenosphere ($T_p = 1280°C$); a mantle plume ($T_p >> 1280°C$); or metasomatized sub-continental lithosphere. Generation of melt in what is, in most respects, a typical continental rift setting has been discussed by many authors in terms of the possible mechanisms of:

(1) Melting of "normal" asthenosphere by adiabatic decompression of upwelling peridotite during rifting.

(2) Melting of mantle plume asthenosphere by adiabatic upwelling.

(3) Melting of metasomatized lithosphere by perturbation of the geotherm by heat from upwelling asthenosphere or a mantle plume.

The first option was the subject of a recent study by McKenzie and Bickle (1988) who demonstrated that a stretching factor (unstretched/stretched ratio) of about 2.5 would be required to melt asthenosphere with a potential temperature of 1280°C and that melting would begin at about 50 km depth (Fig. 10). This is a most improbable scenario for the Arabian foreland because of the positive topographic expression and the geometrical problems that a stretching factor of 2.5 would entail. The second option, the mantle plume, would enable melting to start at greater depth (100 km at a potential temperature of 1480°C) and would better explain the local topography. However there are many arguments against a plume origin for volcanism in Eastern

Anatolia, at least in the sense of the typical plume described by White and McKenzie (1989) as a narrow (150 – 200 km) central plume spreading out to give a mushroom-shaped hot region 1000 – 2000 km in diameter and producing dynamic uplift over the centre of the plume and isostatic uplift over an area 1000 – 2000 km in diameter. The main arguments are:

(1) In Eastern Anatolia the overall volcanic expression is asymmetric, extending about 300 km in the direction of compression and 900 km (into Iran) perpendicular to the direction of compression.

(2) The topographic expression is consistent with north – south shortening rather than domal uplift.

(3) There is a predominance of strike-slip and compressional, rather than extensional, fault-plane solutions.

(4) The temporal changes in volcanic activity over the last 6 Ma show a trend from more regional-scale activity (the early creation of the Kars Plateau in the north and the Mus – Solhan volcanosedimentary units in the south) to localized activity in an aligned set of central vent volcanoes; this is the reverse of that observed in the early stages of plume-related volcanic activity.

(5) The systematic changes in lava chemistry across the collision zone indicate a number of spatially-distinct magma sources, inconsistent with a plume being a source of magma (though not of heat).

We therefore consider the mantle lithosphere must be the dominant, and probably the only, source of magma and that volcanism in the foreland is not the marginal expression of a mantle plume. The volcanism could be explained by some other type of thermal perturbation of the asthenosphere, but the quasi-linear SW – NE trend of much of the youngest volcanism from the foreland to Soviet Armenia suggests a response to localized stretching, perhaps due to the lateral stress release associated with the escape of the Anatolian and Iranian microplates, reducing the angularity of the Eurasian margin into which the Arabian plate is being indented (Sengör, 1976).

A number of studies have been made of lithospheric melting in continental extension (e.g. Latin et al., 1990; Hawkesworth and Norry, 1982; Menzies and Hawkesworth, 1987). The basic requirement is a perturbation of the lithosphere geotherm due to upwelling of hot asthenosphere either by stretching of lithosphere (e.g. Dixon et al., 1981) or an increase of asthenosphere temperature which then brings the metasomatized "layer" above its solidus. Since the metasomatized mantle could lie just below its solidus (especially if the metasomatism resulted from solidification of melt intersecting its solidus), little perturbation may be necessary to initiate melting. Thus, small degrees of stretching may have created the foreland volcanic event, and this is consistent with the absence of topographic evidence for extensive stretching and the geochemical evidence for small degrees of melting put forward earlier.

Volcanism between the Bitlis Thrust Zone and Erzurum

The lavas from this central part of the collision zone have been shown to: (1) vary from transitional (Bingöl, Süphan) through mildly alkaline (Mus, Nemrut) to strongly alkaline (Tendürek); (2) range from basalts, through trachyandesites and trachytes to rhyolites and phonolites; (3) have anhydrous fractionation phases (with the possible exception of Bingöl and Süphan); (4) have trace element and isotope ratios which indicate an enriched mantle source (relative to "normal" asthenosphere), containing no subduction component in the alkaline volcanoes of Mus, Tendürek and Nemrut and a probable subduction component in the cases of Bingöl and Süphan; and (5) have experienced significant but variable crustal contamination before eruption.

In order to understand magma genesis in the

zone of thickened lithosphere north of the foreland, we can take as a starting point the $P-T$ relationships of mineral stabilities, solidi and geothermal gradients for the simple case of instantaneous homogeneous thickening of the mantle lithosphere by 50%, corresponding to the apparent proportional increase in crustal thickness in Eastern Anatolia (Fig. 11b). Several effects are apparent, one being the production of a 50% increase in the thickness of the metasomatized layer. In addition, the metasomatized layer will be depressed below the amphibole breakdown curve, forming garnet and releasing water which can react to form phlogopite or, at the inflection of the solidus, may initiate melting. The lowering of the geotherm will, however, mean that most of the metasomatized layer will lie significantly below the solidus.

To some extent, the same types of constraint on magma genesis apply here as in the case of unthickened lithosphere. We therefore reject the possibility of asthenospheric melting for similar reasons as presented in the case of the foreland: the topographic expression and volcanic evolution of the region are inconsistent with a mantle plume beneath Eastern Anatolia; and melting of normal upwelling asthenosphere is even less likely since even greater stretching factors are now required before the asthenosphere intersects its solidus (a factor of 3.75 would be required for melting of dry asthenosphere rising from the base of the thickened lithosphere). Again, therefore, we can consider the lithosphere as the dominant, or sole, source of magma.

Although simple perturbation of the lithosphere as described earlier could initiate melting of the thickened litosphere, a much more effective mechanism would be the delamination of the TBL. It has been argued that the thickened TBL, being colder and denser than its surroundings, could be convectively replaced by asthenosphere (Houseman et al., 1981; England and Houseman, 1988), causing asthenosphere to be brought into close contact with the thickened layer of metasomatized lithosphere. Relaxation to the perturbed geotherm (G_{pert}) in Figure 11b can then bring a substantial portion of the metasomatized lithosphere above its solidus. Such a process could also be accompanied by the other mechanisms of stretching that characterize thickened lithosphere, notably the creation of pull-apart basins associated with continental escape strike-slip faults. The extensional deviatoric stress perpendicular to the principal direction of compression caused by the potential energy contrast between the elevated region and its surroundings (England and McKenzie, 1983; Houseman and England, 1986) may also have some effect. Uplift of the thickened terrain will also bring the metasomatized lithosphere nearer to its solidus.

If delamination of the TBL is a prime cause of melting of the thickened lithosphere, the details of melting will depend on the time scale of the convective thinning, which, according to Houseman et al. (1981), could take place on a time scale of a few to a few tens of millions of years after thickening. If delamination is a catastrophic rather than continuous event, with the TBL being replaced rapidly (the time scale of crustal thickening and thermal re-equilibration of the lithosphere), then Figure 11b will still apply, although the lithosphere may not have reached its full thickness by the time delamination takes place. When this does happen, the consequences should be a rapid increase in surface elevation (England and Houseman, 1988) which would be about 1 km for Eastern Anatolia. In the EACZ, there are insufficient data on the uplift history to make any precise interpretations. As discussed earlier, initiation of rapid uplift is likely to have taken place at about 12 Ma, with initiation of the main volcanic event (including the Kars Plateau) at about 6 Ma and initiation of the NW – SE chain of stratovolcanoes at about 2 Ma. Such a chronology would be consistent with a delamination event starting at about 6 Ma with the initiation of volcanism and uplift

of the Kars Plateau; the NW – SE chain of stratovolcanoes could then result from subsequent localized extension associated with continental escape. It is, however, beyond the scope of this paper to attempt a more detailed justification of this possibility, which in any case requires more regional geophysical information on the current lithospheric structure and mantle dynamics.

The effect on the crustal part of the geotherm is also significant in magma genesis but will depend on the nature of the thickening event and the relative importance of thrusting and homogeneous thickening (England and Thompson, 1986). Intracrustal melting can theoretically take place during thrusting, possibly by fluid release into the hot base of the overlying thrust sheet. Given sufficient time, radioactive heating can eventually cause dry melting at the base of the crust. Not knowing the precise history of crustal thickening, it is impossible to model the crustal geotherm in the EACZ but it is likely that heating of thickened crust is important in explaining the extent of crustal assimilation in the thickened zone; there is no evidence for pure crustal melting in the EACZ.

Ararat – Kars volcanism

The lavas from this central part of the collision zone have been shown to: (1) have calc-alkaline compositions; (2) belong to the basalt – andesite – dacite – rhyolite fractionation series; (3) show evidence of extensive hornblende crystallization at depth prior to plagioclase, two-pyroxene crystallization in shallow magma chambers; (4) have trace element and isotope ratios which indicate a slightly enriched mantle source containing a significant subduction component. These characteristics could be caused by active subduction or be inherited from an earlier subduction event. Innocenti et al. (1982b), who first recognized the chemical zonation across the collision zone, proposed that the splitting of underlying subducted lithosphere would allow the regions above the subducted lithosphere to have a calc-alkaline composition, whereas those above the split would have alkaline compositions. We reject this model, on the same grounds as those put forward by Yilmaz (1990), because there are no intermediate- or deep-focus earthquakes in the EACZ, and thus agree with Yilmaz that the differences lie in inherited lithospheric characteristics. The Kars – Ararat calc-alkaline domain in the north would then be expected to coincide with the lithosphere of the Pontides which has experienced subduction for at least part of the period from the late Cretaceous to the middle Eocene: the forearc lithosphere on which the Kars – Ararat province would be located should be especially enriched. The source of the calc-alkaline component in the Bingöl – Süphan region is less obvious: it may be derived from the forearc lithosphere of a short-lived Eocene subduction event adjacent to the Bitlis Massif. If so, it may be possible to investigate the mixing of two distinct lithospheric sources: the underthrust Arabian lithosphere and the Anatolian lithosphere. Alternatively, it may be a long-lived, inherited characteristic of the Arabian lithosphere.

The contrast between the calc-alkaline and alkaline volcanism also provides the opportunity to contrast the melting of metasomatized mantles with different H_2O/CO_2 ratios. Figure 11b shows the thickened lithospheric section upon which have been superimposed the solidi for pure water and pure carbon dioxide (Wyllie, 1987). At the likely depths of melting of thickened lithosphere (> 100 km), both solidi should increase with pressure, but the H_2O-rich mantle will melt at lower temperatures. In both cases, the greatest volume of melt for a given heat input would be generated at a depth of about 100 km where both solidi are at their lowest temperatures after breakdown of amphibole and magnesite respectively. If latent heat considerations determine the amount of melt generated at a given depth, the calc-alkaline magmas should be lower temperature magmas that have

undergone more melting. This may account for the significantly greater volume of magma erupted in the early stages of magmatism to form the Kars Plateau compared to the Mus region and explain the ability of the Kars – Ararat magmas to crystallize amphiboles at an early stage.

One tectonic implication of these findings might be that the Pontide Suture Zone lies between Tendürek, where anhydrous volcanics are erupted, and Ararat the most southerly location of the Kars – Ararat belt of hydrous volcanic rocks.

Conclusions

The combination of petrological and geochemical and tectonic constraints have enabled us to propose the model illustrated in Figure 12 for magma genesis within the Eastern Anatolian Collision Zone. The main aspects of this model, and their justifications, are briefly summarized below:

(1) Because of the thermal constraints in melting the convecting upper mantle and the weight of evidence against a mantle plume origin, volcanism across the Eastern Anatolian Collision Zone (EACZ) can be inferred to be caused by thermal perturbation of metasomatized subcontinental lithosphere. The likely mechanisms are the delamination of the thermal boundary layer, or localized extension, or both. Thickening of the sub-continental lithosphere could have the effect of thickening the metasomatized layer and depressing it to greater depths, below the amphibole and dolomite breakdown curves. Compatible – incompatible element covariations indicate that the degree of partial melting was lower in the unthickened litosphere of the foreland than in the lithosphere of the thickened zone.

(2) Systematic variations in petrologic and geochemical characteristics across the province reflect variations in the enrichment history of the various lithospheric domains. In the Arabian foreland, the absence of any LIL element-rich subduction component suggests that its mantle lithosphere may have experienced a time-integrated metasomatism, by low-degree melts from the asthenosphere, from the late Precambrian "Pan-African orogeny" to the present day. A similar source is required by the Mus – Nemrut and Tendürek regions of the thickened zone: this could be the same, under-

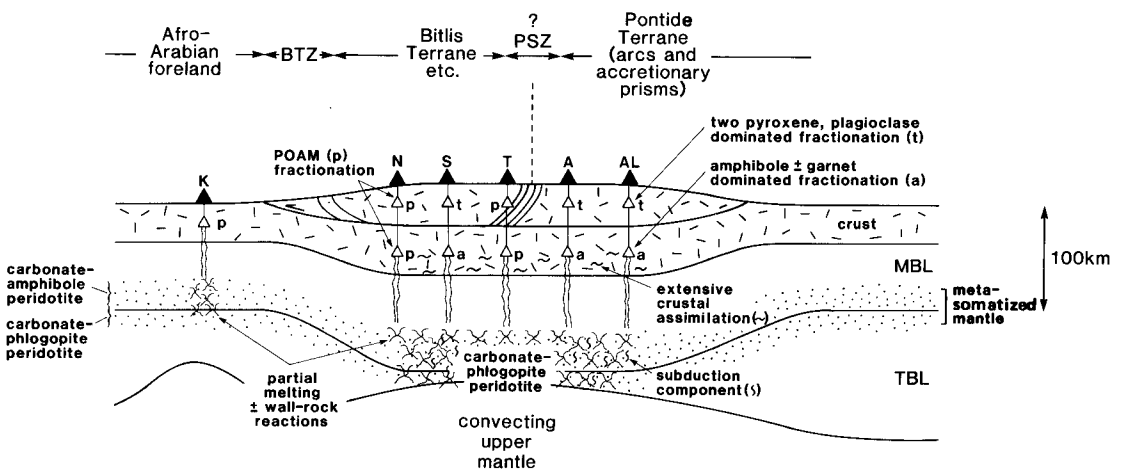

Fig. 12. Schematic section across the Eastern Anatolian volcanic province summarizing the magmaggenetic model deduced from petrological and geochemical data. *PSZ* = Pontide Suture Zone; *N* = Nemrut; *S* = Süphan; *T* = Tendürek; *A* = Ararak; *AL* = Aladag.

thrust Arabian mantle lithosphere and/or the mantle lithosphere of the Bitlis Massif microcontinent. By contrast, the consistent, regional enrichment in LIL elements across the Kars – Ararat province in the north of the thickened zone suggests that the lithosphere of this province was enriched by fluids and melts during the late Cretaceous – Eocene Pontide subduction event. Ararat thus has a volcanic arc chemistry but not an arc setting (although it may have had an ark setting!). The similar enrichment in the Süphan – Bingöl province is less easy to explain, but may also be related to a short-lived Eocene – Miocene subduction event that may have taken place adjacent to the Bitlis Massif in the south.

(3) Although the studies of Innocenti et al. (1976, 1980, 1982b) have suggested that the earliest volcanism was calc-alkaline and that this was followed by alkaline volcanism, our work does not support such an interpretation. We note, in particular, that the Kars Plateau (7 – 1.5 Ma) and Ararat (1.5 – < 0.5 Ma) have almost identical, calc-alkaline, mineralogical and geochemical characteristics. Similarly the Mus region (> 6 – < 4 Ma) and Nemrut (1 – 0 Ma) in the south of the thickened zone have almost identical mildly alkaline characteristics; and Bingöl (> 4 – < 3 Ma) and Süphan (1.5 – 0.2 Ma) have similarly transitional characteristics. Thus, although more data are needed from the older volcanic sequences, this work suggests that the region is characterised by a set of mantle domains running parallel to the collision zone, each of which has yielded magmas of a particular composition since the start of magmatism in the region. We also question the previous ideas on the timing of the start of volcanism. Early Miocene dates are extremely rare, and our studies of early volcanism in the Mus area give dates of 6 – 4 Ma. On the basis of information currently available, we would therefore favour a start of post-collision volcanism at about 8 – 6 Ma following the start of major uplift at about 12 Ma. The age of initiation of the collision itself is more contentious, as discussed in the introductory sections. It cannot be younger than 12 Ma and, in our view, is unlikely to be much older than 20 Ma. However, as there is no direct volcanic or plutonic evidence of post-Eocene subduction in the EACZ it is possible that collision may have begun as long ago as 40 Ma.

(4) Evidence, from Kars and Ararat in particular, demonstrates the operation of polybaric crystallization. Lavas from this province contain anhydrous crystallization assemblages (mainly two pyroxenes and plagioclase) yet trace element characteristics (such as Y, M – HREE and Nb depletion are indicative of extensive amphibole crystallization at an early stage of crystallization: phase diagrams confirm that low-temperature hydrous magmas can crystallize liquidus or near-liquidus amphibole at lower crustal depths but anhydrous assemblages at shallower depths.

(5) Isotope – trace element systematics indicate that combined assimilation – fractional crystallization is an important process in the thickened crust south of Ararat. There is no good evidence for significant assimilation in the Kars – Ararat region, but this may be due to the lack of chemical contrast between the magmas and the likely young, calc-alkaline crust of the Pontide Terrane. Increased lower crustal temperatures resulting from thermal relaxation of the thickened crust will have favoured extensive crustal assimilation in the thickened zone.

(6) If we are correct in assuming that the collision-related magmas all originate in variably enriched mantle lithosphere, the distribution of the volcanism in space and time on the Eastern Anatolian Plateau has implications for the scale and timing of delamination of thickened mantle lithosphere. Because there is no systematic age progression of volcanism across or along the thickened zone north of the Bitlis Thrust Zone, we can infer that delamination must have simultaneously affected the whole thickened zone, either as a succession of small-scale detatchments or a single, catastrophic

detatchment. Further studies of the uplift history of the region may help to resolve these two options.

Acknowledgements

JAP carried out this work with the aid of a Royal Society of London Overseas Travel Grant and PJL a Natural Environment Research Council Research Studentship. We are grateful to Gareth Davies, Philip Leat, Peter Oakley, Ron Hardy and Paul Laverick for assistance and advice on isotope. INAA, AA and XRF analyses, respectively. SED and WSFK were supported by National Science Foundation grant EAR – 7904887. WSFK, SED, YG, FS and YY gratefully acknowledge logistic support from the MTA and, in particular the directors of the Van and Diyabakir offices of MTA. We thank Mehmet Keskin, Dave Latin, Nick Rogers, Matthew Thirlwall and Rob Westaway for their helpful comments on the manuscript, and Phil England for providing a preprint of his work on the mechanics of continent collisions.

References

Ambraseys, N.N., 1970. Some characteristic features of the Anatolian Fault Zone. Tectonophysics, 9: 143 – 165.

Autio, L.K. and Rhodes, J.M., 1983. Costa Rica rift zone basalts: geochemical and experimental data from a possible example of multi-stage melting. Init. Rep. DSDP 69: 729 – 745.

Bailey, D.K., 1987. Mantle metasomatism – perspective and prospect. Geol. Soc. London, Spec. Publ., 30: 1 – 13.

Bender, J.F., Langmuir, C.H. and Hanson, G.N., 1984. Petrogenesis of basalt glasses from the Tamayo region, East Pacific Rise. J. Petrol., 25: 213 – 254.

Brinkmann, R., 1976. Geology of Turkey. Ferdinand Enke, Stuttgart, 158 pp.

Carlson, R.W., Lugmair, G.W. and MacDougall, J.D., 1981. Columbia River volcanism: the question of mantle heterogeneity or crustal contamination. Geochim. Cosmochim. Acta, 45: 2483 – 2499.

De Paolo, D.J., 1981. Trace element and isotopic effects of combined wall rock assimilation and fractional crystallization Earth Planet. Sci. lett., 53: 189 – 202.

Dewey, J.F., Hempton, M.R., Kidd, W.S.F., Saroglu, F. and Sengör, A.M.C., 1986. Shortening of continental lithosphere: the neotectonics of Eastern Anatolia – a young collision zone. In: M.P. Coward and A.C. Ries (Editors), Collision Tectonics. Geol. Soc. London, Spec. Publ., 19: 3 – 36.

Dixon, J.E., Fitton, J.G. and Frost, R.T.C., 1981. The tectonic significance of post-Carboniferous igneous activity in the North Sea basin. In: L.V. Illing and G.D. Hobson (Editors), Petroleum Geology of the Continental Shelf of North West Europe. Blackwell, London, pp. 29 – 52.

England, P.C. and Houseman, G.A., 1988. The mechanics of the Tibetan Plateau. Philos. Trans. R. Soc. London, A326: 301 – 320.

England, P.C. and McKenzie, D.P., 1983. A thin viscous sheet model for continental deformation. Geophys. J.R. Astron. Soc., 73: 523 – 532.

England, P.C. and Thompson, A., 1986. Some thermal and tectonic models for the crustal melting in continental collision zones. In: M.P. Coward and A.C. Ries (Editors) Collision Tectonics. Geol. Soc. London, Spec. Publ. 19: 83 – 94.

Faure, G., 1986. Principles of Isotope Geology. Wiley, New York, 589 pp.

Gealy, W.K., 1977. Ophiolite obduction and geologic evolution of the Oman mountains and adjacent areas. Geol. Soc. Am. Bull., 88: 1183 – 1191.

Gill, J.B., 1981. Orogenic Andesites and Plate Tectonics. Springer, Berlin, 390 pp.

Green, T.H., 1982. Anatexis of mafic crust and high pressure crystallization of andesite. In: R.S. Thorpe (Editor), Orogenic Andesites. Wiley, Chichester, U.K., pp. 465 – 487.

Gülen, L., 1980. Strontium isotope geochemistry of Mount Ararat and Mount Süphan volcanics, Eastern Turkey. Eos, Trans. Am. Geophys. Union, 61: 412. (Abstr.)

Gülen, L., 1982. Sr, Nd and Pb systematics of Ararat and Süphan volcanoes, Eastern Turkey. Eos, Trans. Am. Geophys. Union, 63: 1145 (Abstr.).

Hall, R., 1976. Ophiolite emplacement and the evolution of the Taurus suture zone, southeastern Turkey. Geol. Soc. Am. Bull., 87: 1078 – 1088.

Hallam, A., 1976. Geology and plate tectonics interpretation of the sediments of the Mesozoic radiolarite – ophiolite complex in the Neyriz region, southern Iran. Geol. Soc. Am. Bull., 87: 47 – 52.

Hawkesworth, C.J. and Norry, M.J., 1982. Continental Basalts and Mantle Xenoliths. Shiva, Cheshire, U.K.

Hempton, M.R., 1982. The North Anatolian Fault and complexities of continental escape. J. Struct. Geol., 4: 502 – 504.

Hempton, M.R. and Dewey, J.F., 1983. Earthquake induced deformational structures in young lacustrine sediments, East Anatolian Fault, southeast Turkey. Tectonophysics, 98: 7 – 14.

Hervig, R.L., Smith, J.V. and Dawson, J.B., 1986. Lherzolite xenoliths in kimberlites and basalts: petrogenetic and crystallochemical significance of some minor and trace elements in olivine, pyroxenes, garnet and spinel. Trans. R. Soc. Edinburgh, Earth Sci., 77: 181 – 201.

Hildreth, W. and Moorbath, S., 1988. Crustal contributions to arc magmatism in the Andes of Southern Chile. Contrib. Mineral. Petrol., 98: 455 – 489.

Houseman, G.A. and England, P.C., 1986. Finite strain calculations of continental deformation. 1, Method and general results for convergent zones. J. Geophys. Res., 86: 6115 – 6132.

Houseman, G.A., McKenzie, D.P. and Molnar, P., 1981. Convective instability of a thickened boundary layer and its relevance for the thermal evolution of continental convergent belts. J. Geophys. Res., 86: 6115 – 6132.

Innocenti, F., Mazzuoli, R., Pasquare, G., Radicati di Brozolo, F. and Villari, L., 1976. Evolution of volcanism in the area of interaction between the Arabian, Anatolian and Iranian plates (Lake Van, Eastern Turkey). J. Volcanol. Geotherm. Res., 1: 103 – 112.

Innocenti, F., Mazzuoli, R., Pasquare, G., Serri, G. and Villari, L., 1980. Geology of the volcanic area north of Lake Van (Turkey). Geol. Rundsch., 69: 292 – 322.

Innocenti, F., Manetti, P., Mazzuoli, R., Pasquare, G. and Villari, L., 1982a. Anatolia and northwestern Iran. In: R.S. Thorpe (Editor), Andesites: Orogenic Andesites and Related Rocks. Wiley, New York, pp. 327 – 349.

Innocenti, F., Mazzuoli, R., Pasquare, G., Radicati di Brozolo, F. and Villari, L., 1982b. Tertiary and Quaternary volcanism of the Erzurum – Kars area (Eastern Turkey): geochronological data and geodynamic evolution. J. Volcanol. Geotherm. Res., 13: 223 – 240.

Irvine, T.N. and Barager, W.R.A., 1971. A guide to the chemical classification of the common volcanic rocks. Can. J. Earth Sci., 8: 523 – 548.

Irving, A.J., 1978. A review of experimental studies of crystal/liquid trace element partitioning. Geochim. Cosmochim. Acta, 42: 743 – 770.

Irving, A.J. and Frey, F.A., 1984. Trace element abundances in megacrysts and their host basalts: constraints on partition coefficients and megacryst genesis. Geochim. Cosmochim. Acta, 48: 1201 – 1221.

Jackson, J. and McKenzie, D.P., 1984. Active tectonics of the Alpine – Himalayan Belt between western Turkey and Pakistan. Geophys. J.R. Astron. Soc., 77: 185 – 264.

Ketin, I., 1976. Main orogenic events and palaeogeographic evolution of Turkey. M.T.A. Bull., 88: 1 – 4.

Lambert, I.B. and Wyllie, P.J., 1970. Low velocity zone of the earth's mantle: incipient melting caused by water. Science, 169: 764 – 766.

Lambert, R.S.J., Holland, J.G. and Owen, P.F., 1974. Chemical petrology of a suite of calc-alkaline lavas from Mt. Ararat, Turkey. J. Geol., 82: 419 – 438.

Latin, D.M., Dixon, J.E. and Fitton, J.G., 1990. Rift-related magmatism in the North Sea basin. In: D.J. Blundell and A. Gibbs (Editors), Tectonic Evolution of the North Sea Rifts. Oxford Univ. Press. (in press).

Leat, P.T., Morrison, M.A. and Trayhorn, S.C., 1987. Geodynamic significance of post-Variscan instrusive and extrusive potassic magmatism in southwest England. Trans. R. Soc. Edinburgh, Earth Sci., 77: 349 – 360.

Le Bas, M.J., Le Maitre, R.W., Streckeisen, A. and Zanettin, B., 1986. A chemical classification of volcanic rocks based on the total alkali – silica diagram. J. Petrol., 27: 745 – 750.

Le Fort, P., 1986. Metamorphism and magmatism during the Himalayan collision. In: M.P. Coward and A.C. Ries (Editors), Collision Tectonics. Geol. Soc. London Spec. Publ., 19: 159 – 172.

McCulloch, M.T. and Chappell, B.W., 1982. Nd isotopic characteristics of S- and I-type granites. Earth Planet. Sci. Lett., 58: 512 – 564.

McKenzie, D.P., 1972. Active tectonics of the Mediterranean region. Geophys. J.R. Astron. Soc., 30: 109 – 185.

McKenzie, D.P., 1976. The East Anatolian Fault: a major structure in eastern Turkey. Earth. Planet. Sci. Lett., 29: 189 – 193.

McKenzie, D.P. and Bickle, M.J., 1988. The volume and composition of melt generated by extension of the lithosphere. J. Petrol., 29: 625 – 679.

Menzies, M.A. and Hawkesworth, C.J., 1987. Mantle Metasomatism. Academic Press, London.

Michard, A., Whitechurch, H., Ricou, L.E., Montigny, R. and Yazgan, E., 1984. Tauric subduction (Malatya – Elazig provinces) and its bearing on tectonics of the Tethyan realm in Turkey. In: A.H.F. Robertson and J.E. Dixon (Editors), The Geological Evolution of the Eastern Mediterranean. Blackwell, Oxford, pp. 361 – 373.

Miyashiro, A., 1974. Volanic rock series in island arcs and active continental margins. Am. J. Sci., 274: 321 – 355.

Nowroozi, A.A., 1972. Focal mechanism of earthquakes in Persia, Turkey, west Pakistan and Afghanistan and plate tectonics of the Middle East. Bull. Seismol. Soc. Am., 62: 832 – 850.

Olafsson, M. and Eggler, D.H., 1983. Phase relations of

amphibole, amphibole – carbonate and phlogopite – carbonate: petrologic constraints on the asthenosphere. Earth Planet. Sci. Lett., 64: 305 – 315.

Ottonello, G., Ernst, W.G. and Joron, J.L., 1984. Rare earth and 3d transition element geochemistry of peridotitic rocks: I. Peridotites from the Western Alps. J. Petrol., 25: 343 – 372.

Pearce, J.A., 1982. Trace element characteristics of lavas from destructive plate margins. In: R.S. Thorpe (Editor), Andesites: Orogenic Andesites and Related Rocks. Wiley, New York, pp. 525 – 548.

Pearce, J.A., 1983. Role of the sub-continental lithosphere in magma genesis at active continental margins. In: C.J. Hawkesworth and M.J. Norry (Editors), Continental Basalts and Mantle Xenoliths. Shiva, Cheshire, U.K., pp. 230 – 249.

Pearce, J.A. and Norry, M.J., 1979. Petrogenetic implications of Ti, Zr, Y, and Nb variations in volcanic rocks. Contrib. Mineral. Petrol., 69: 33 – 47.

Pearce, J.A., Rogers, N., Tindle, A. and Watson, J., 1986. Geochemistry and petrogenesis of basalts from DSDP Leg 92. Init. Rep. DSDP 92: 729 – 745.

Peccerillo, A. and Taylor, S.R., 1976. Geochemistry of Eocene calc-alkaline volcanic rocks from the Kastamonu area, Northern Turkey. Contrib. Mineral. Petrol., 58: 63 – 91.

Robertson, A.H.F. and Aktas, A.H.F., 1984. The Maden Complex, SE Turkey: evolution of a neotethyan active margin. In: A.H.F. Robertson and J.E. Dixon (Editors), The Geological Evolution of the Eastern Mediterranean, Blackwell, Oxford, pp. 375 – 402.

Rotstein, Y. and Kafka, A.L., 1982. Seismotectonics of the southern boundary of Anatolia, eastern Mediterranean region: subduction, collision and arc jumping. J. Geophys. Res., 87: 7694 – 7706.

Sanver, M., 1968. A palaeomagnetic study of Quaternary volcanic rocks from Turkey. Phys. Earth Planet. Inter. 1: 403 – 421.

Saroglu, F., Güner, Y., Kidd, W.S.F. and Sengör, A.M.C., 1980. Neotectonics of Eastern Turkey: new evidence for crustal shortening and thickening in a collision zone. Eos, Trans. Am. Geophys. Union, 61: 360 (Abstr.).

Sengör, A.M.C., 1976. Collision of irregular continental margins: Implications for foreland deformation of Alpine-type orogens. Geology, 4: 779 – 782.

Sengör, A.M.C. and Kidd, W.S.F., 1979. Post-collisional tectonics of the Turkish-Iranian plateau and a comparison with Tibet. Tectonophysics, 55: 361 – 376.

Sengör, A.M.C. and Yilmaz, Y., 1981. Tethyan evolution of Turkey: a plate tectonic approach. Tectonophysics, 75: 181 – 241.

Tatar, Y., 1975. Tectonic structures along the North Anatolian Fault Zone, north west of Retahiye (Erzincan). Tectonophysics, 29: 401 – 410.

Taylor, S.R. and McLennan, S.M., 1985. The Continental Crust: its Composition and Evolution. Blackwell, Oxford, 312 pp.

Tchalenko, J.S., 1977. A reconnaissance of the seismicity and tectonics at the Northern border of the Arabian plate (Lake Van region). Rev. Géogr. Phys. Géol. Dyn., 19: 189 – 208.

Töksöz, M.N., Arpat, E. and Saroglu, F., 1977. East Anatolian earthquake of 24 November 1976. Nature, 270: 423 – 425.

White, R. and McKenzie, D.P., 1989. Magmatism at rift zones: the generation of volcanic continental margins and flood basalts. J. Geophys. Res., 94: 7685 – 7729.

Wilkinson, P., Mitchell, J.G., Cattermole, P.J. and Downie, C., 1986. Volcanic chronology of the Meru – Kilimanjaro region, Northern Tanzania. J. Geol. Soc. London, 143: 601 – 603.

Wyllie, P., 1987. Metasomatism and fluid generation in mantle xenoliths. In: P.H. Nixon (Editor), Mantle Xenoliths. Wiley, Chichester, U.K., pp. 609 – 621.

Yilmaz, Y., 1990. Comparisons of the young volcanic associations of Western and Eastern Anatolia under the compressive regime. J. Volcanol. Geotherm. Res. (in press).

Yilmaz, Y., Saroglu, F. and Güner, Y., 1987. Initiation of the neomagmatism in East Anatolia. Tectonophysics, 134: 177 – 199.